Infrared matrix- isolation and theoretical studies of interactions between CH3I and water

Sophie Sobanska, Hanaa Houjeij, Stéphane Coussan, Christian Aupetit, Sonia Taamalli, Florent Louis, Laurent Cantrel, Anne Cecile Gregoire, Joelle Mascetti

Infrared matrix-isolation and theoretical studies of interactions between CH_3I and water

Sophie Sobanska[1]*, Hanaa Houjeij[1,4], Stéphane Coussan[2], Christian Aupetit[1], Sonia Taamalli[3], Florent Louis[3], Laurent Cantrel[4], Anne Cécile Gregoire[4], Joëlle Mascetti[1]

1- Institut des Sciences Moléculaires, Université de Bordeaux, UMR5255 CNRS, 33405 Talence cedex, France

2- CNRS, Aix-Marseille Univ, PIIM, Marseille13397, France

3- Physico-Chimie des Processus de Combustion et de l'Atmosphère, Université de Lille, UMR8522 CNRS, 59000 Lille, France

4- Institut de Radioprotection et de Sûreté Nucléaire, IRSN/PSN-RES, Cadarache, 13115 St Paul Lez Durance, France

*corresponding author: sophie.sobanska@u-bordeaux.fr

Abstract

Gaseous iodomethane are naturally emitted in the atmosphere over oceans through the algae and phytoplankton activities. The fate of naturally emitted iodomethane is of great interest because of the oxidizing properties of iodine in the atmosphere and its impact on the catalytic destruction of the ozone layer. Additionally, iodomethane is one of the gaseous species that can be emitted in the case of severe nuclear accident. The radiological impact of gaseous iodomethane is of concerns and requires knowledge about its behavior in the atmosphere. Water is one of the major species in the atmosphere which is responsible for atmospheric aerosol nucleation and thus, for cloud condensation nuclei (CCN). The fundamental knowledge concerning the interaction between methyl iodine and water at the molecular scale contributes to the better understanding of the fate of such species into the atmosphere and their role in CCN formation. Here the microhydration of iodomethane was investigated using cryogenic matrix experiments which were supported by theoretical DFT calculations. A large excess of water regarding CH_3I was used in order to mimic atmospheric conditions. Dimers and trimers of CH_3I are observed despite the high water amount in the initial mixture together with hetero aggregates between CH_3I and water clusters. This may be explained by the low affinity of CH_3I with water. Considering the concentration of iodomethane used in our experiments, the aggregates are rather formed in gas phase and not in the matrix cage. The interaction between CH_3I and H_2O molecules studied experimentally and supported by DFT calculation highlights that, in the

atmosphere, gaseous iodomethane and water will likely form association between water and iodomethane aggregates instead of $(CH_3I)_n$-$(H_2O)_m$ hetero complexes. Our results have important consequences for the understanding of the alkyl halide solvation in primary processes and contribute to the understanding of reactive halogen species in tropospheric chemistry. In the context of a nuclear severe accident, our work is contributing to better understand the fate of nuclear species in the atmosphere and thus, the radionuclide dispersion.

Key words: iodomethane, hydration, nuclear accident, atmosphere, matrix isolation infrared spectroscopy

1. Introduction

Iodine is an important fission product of the fuel used in Nuclear Power Plants (NPPs) in terms of safety with the generation of high radioactive isotopes (^{131}I and ^{133}I) potentially released outside in case of severe accident. Indeed, radioactive gaseous iodine poses a health hazard if released into the atmosphere due to its accumulation in the human thyroid gland after inhalation, where it can locally induce cancer [1-4]. A severe accident in a NPPs as Chernobyl (Ukraine) and the more recent Fukushima- Daichi (Japan) disaster can led to gaseous molecular iodine (I_2) and methyl iodide (CH_3I), as main representative of organic iodides released into the atmosphere [5-7]. Particularly, it has been postulated that the removal of CH_3I with the currently used filter materials (for instance as charcoal media or liquid scrubber) is less efficient compared to I_2 [3,8,9]. Hence, the reactivity of CH_3I in the atmosphere has recently gained much interest in the field of nuclear industrial safety as its interaction with atmospheric species i.e. gaseous oxidants, radicals, water or aerosols may influence the atmospheric dispersion and thus the sanitary impacts.

Iodine also occurs naturally in the ocean boundary layer and is mainly derived from algae and phytoplankton in the oceans and from heterogeneous reactions at the ocean-atmosphere interface [10-12]. The iodine species mainly emitted by these natural sources are halogenated organic compounds such as CH_3I. The atmospheric chemistry of iodine species is of great interest because of the oxidizing properties of iodine in the atmosphere and its impact on the catalytic destruction of the ozone layer. The chemistry of halogens especially the marine iodine chemistry has been extensively studied and was reviewed by Saiz-Lopez et al. [11] and Simpson et al. [12]. These previous works mainly focus on gaseous chemistry and photochemistry of iodine species such as CH_3I which leads to the formation of iodine oxide particles (IOP). Iodine oxide-driven new particle formation has been reported from both field observations and

laboratory experiments. As one of the main species present in the atmosphere, water molecules may affect the reactivity of the gaseous species. As a gas, water molecules may form some aggregates or complexes with atmospheric species. As a liquid droplet, water may dissolve gaseous components, the latter being driven by Henry's law constant [13,14]. Recently, the microhydration of n-alkyl halides has received much attention as it may affect the halide chemistry processes such as photolysis, and more generally the atmospheric halide cycle. The atmospheric gas-to-particle conversion mechanism may be also influenced by the humidity as it is reported for the IOP formation. Additionally, the effect of water on aerosol chemical processes are increasingly questioned [15 and reference herein] since water cluster growth and further, hygroscopicity properties of aerosols, are the most research concerns for understanding the cloud formation. The interaction between water and halide compounds (including iodine) has been mainly investigated using ab initio calculations [16 and ref herein] since sparse experimental data are available due to the challenging task to study water-alkyl interaction in ambient conditions. In a previous work, the structure and vibrational spectra of methyl halides dimers has been examined by ab initio calculation [17]. Besides, Ito et al. have studied the formation of CH_3I clusters and CH_3I-H_2O (1:1) complex by using the matrix isolation technique [18-20] since the matrix isolation technique is a relevant experimental technique to study inter- and intra-molecular interactions occurring during the microhydration process. In Ito's papers, the only CH_3I-H_2O complex considered is the 1:1 ratio when complexes with higher number of molecules are expected in the atmosphere. The main question that remains for further atmospheric implication, i.e. the influence of water on both reactivity of halide compounds in gaseous phase and CCN formation, is: in the atmospheric conditions i.e. with high water content, is CH_3I species able to form complexes $(CH_3I)_n(H_2O)_m$ with water molecules or only aggregates of homo-clusters of $(CH_3I)_n$ and $(H_2O)_m$ can be observed?

In the present paper, we have investigated the interactions between CH_3I and H_2O to give insights on the microhydration process of CH_3I, which in turn help in understanding the reactivity of CH_3I in the gas phase and its molecular interaction with hydrated aerosols. Increasing the knowledge of CH_3I reactivity will contribute to improve the understanding of the atmospheric iodine cycle and consequently, the prediction of the radiological consequences resulting from accidental iodine radioisotope releases. The matrix- isolation Fourier Transform Infra-Red (FTIR) spectroscopy technique was used for studying in details the formation of $(CH_3I)_n$-$(H_2O)_m$ complexes or aggregates of homo-clusters. To help in the interpretation, the formation of $(CH_3I)_n$ clusters were studied in similar experimental conditions and the structure,

infrared spectra and energetics of the observed species have been investigated by Density Functional Theory (DFT) calculations.

2. Experimental and theoretical section

Matrix isolation experiments. The matrix isolation system used in this work has been described in details elsewhere [21-23]. Experiments were conducted in a high vacuum experimental set up consisting in a stainless steel chamber (P= 10^{-5} mbar at room temperature) containing an IR transparent NaCl window cooled to 10K by means of a closed cycle He cryostat Cryophysics Cryodine. The sample temperature is monitored with a Si diode thermometer set on the copper holder of the NaCl window. Two sets of experiments were conducted in this work to scrutinize the CH_3I-H_2O interactions at low temperature (1) CH_3I in Ar matrix from 10 to 35 K as benchmark experiment and (2) CH_3I and H_2O in Ar matrix from 10 to 35 K. Gaseous samples of CH_3I/Ar (0.1% CH_3I - 99.9% Ar, Airproduct) were used without any further purification at a flow of 1mL/min. The matrix ratio is then CH_3I/Ar = 1/1000 since various ratios were investigated in previous work [20]. For the observation of the formation of $(CH_3I)_m$-$(H_2O)_n$ complexes, the vapor of ultrapure H_2O (conductivity of 18.2 MΩ Millipore system) was introduced from a glass flask and mixed with CH_3I/Ar in a glass reservoir in the proportion CH_3I/ H_2O/Ar = 1/25/1500 and injected into the chamber at a rate of 1 mL/min^{-1}. This CH_3I/H_2O ratio is chosen to ensure both high water concentration in matrix and CH_3I signal detection since beyond this ratio, signals of water aggregates would overlap those of $(CH_3I)_m$-$(H_2O)_n$. Deionized water was previously subjected to multiple freeze-pump-thaw cycles under vacuum to remove dissolved gases. Thus, the concentration H_2O/Ar equal to 1/60 introduced was used to mimic the closest atmospheric conditions. A reference experiment with H_2O trapped in Ar matrix (7/1000) was also recorded at 4 K for comparison. The gaseous samples were introduced by gas nozzle inlet and deposited by diffusion directly on NaCl plate for 2 hours. This deposition mode is soft enough to limit cluster formation during the deposition process. The deposited samples at 10 K were annealed to 35 K, close to the sublimation temperature of the argon crystal. The infrared spectra of the gas-isolated samples were recorded in transmission mode using a Bruker Vertex 70V FTIR spectrometer with a DTGS detector in the spectral range 4000-400 cm^{-1}, with a spectral resolution of 0.5 cm^{-1} and each spectrum averaged over approximately 200 scans. Spectra were recorded at 10K for CH_3I and CH_3I/H_2O experiments.

Theoretical Calculations. The structure and harmonic vibrational spectra of CH_3I monomer, dimers and trimers, and CH_3I-water complexes such as $(CH_3I)_m$-$(H_2O)_n$ (with m = 1,2,3 and n

= 1,2,3) were calculated with the Gaussian09 suite of programs |24] using the long range corrected functional ωB97X-D [25] with the aug-cc-pVTZ basis set for hydrogen, carbon and oxygen atoms, while the aug-cc-pVTZ-PP basis set [26] was used for the iodine atom that incorporates a small-core relativistic pseudo potential, as previously mentioned [27]. Harmonic vibrational frequencies have been calculated at the same level of theory, and remained unscaled. Additionally, NBO analysis was performed on the isolated molecules CH_3I and H_2O and on $CH_3I.H_2O$ (1:1a and 1:1b) complexes at the ωB97X-D/aug-cc-pVTZ level of theory. The standard molar entropy ($S°_{10\ K}$) and the heat capacity at constant pressure (1 bar) have been calculated with the script thermo.pl published by the National Institute of Standards and Technology [28]. The Gibbs free energy of reaction ($\Delta_r G^0$) in $kJ.mol^{-1}$ for both CH_3I clusters and complexes have been calculated at the ωB97XD/ aug-cc-pVTZ-PP level of theory. The basis set superposition error (BSSE) correction is known to be negligible in microhydration energetics, [27, 29] therefore this correction has not been included in the energetic calculations of this study.

The IR band assignment was performed by comparing the observed and calculated shifts Δν. The frequency shifts are calculated with respect to the monomer position ($\Delta\nu = \nu - \nu_{monomer}$).

3. Results and discussion

Formation of $(CH_3I)_n$ clusters. Structures of CH_3I monomer, dimers and trimers were investigated using experimental spectra supported by calculations presented above. Two isomers of $(CH_3I)_2$, shown in Fig. S1(a) with xyz coordinates reported in Table S2 (Supporting Information), are found to be stable and will be hereafter referred as Head-to-Tail (HT) and Head-to-Head (HH) structures. These structures were previously reported using the MP2/ LanL2DZ+fdp level of theory [18]. It should be highlighted that both levels of theory using MP2/ LanL2DZ+fdp [18] and ωB97XD/aug-cc-pVTZ-PP (this work) predict the same $(CH_3I)_2$ stable isomers, i.e. HH and HT, with a difference in the intermolecular distance not exceeding 0.2 Å. A Gibbs free energy difference of 3.0 and 3.8 kJ/mol is found for HH and HT isomers respectively, between the method used in this study and the one used previously [18]. Two $(CH_3I)_3$ isomers have also been found to be stable (Fig. S1(b) and Table S2 (SI)) and will be hereafter referred as Tail-to-Head-to-Tail THT_1 and THT_2. The THT_2 structure was previously discussed by Ito et al. [20,30] to be the most stable structure of $(CH_3I)_3$ using the MP2 method. In the present work the Gibbs free energy difference between the 2 isomers is less than 1 kJ/mol at the ωB97X-D/ aug-cc-pVTZ-PP level of theory. As a result, THT_1 and THT_2 could be

considered as isoenergetic. The difference in the intermolecular distance between the level of theory used in this study and the one used previously [30] does not exceed 0.2 Å. Moreover, a difference of about 5 kJ/mol in the Gibbs free energy was found between the two levels of theory. As a result, the difference in binding energies shows that ΔE(ωB97X, this work) is lower than ΔE calculated using MP2 method [18,30] for both CH_3I dimers and trimers. This interaction between CH_3I molecules is more accurately evaluated using the ωB97X-D functional, which is consistent with a recent study [17] that includes dispersion for a better characterization of the inter-molecular complexes under study. Moreover the size of the basis set is larger in our work (aug-cc-pVTZ-PP) than the one used in Ito's studies (LANDZ+fdp) [18,30].

The calculated vibrational spectra together with bands relative intensities of the monomer and the most stable HH, HT, THT_1, THT_2 isomers are gathered in Table S8. For a more reliable analysis of CH_3I clusters infrared spectra, we used unscaled IR frequencies. It should be noted that the calculated wavenumber position is likely dependent of the level of theory. For example, the wavenumber position of the monomer CH_3 symmetric deformation mode is calculated at 1334 cm^{-1} using the MP2/ LanL2DZ+fdp level of theory [18], whereas it is calculated at 1297 cm^{-1} in this work using the ωB97X-D/aug-cc-pVTZ-PP level of theory. It is known that the shift from the monomer peak due to clustering can be evaluated by theoretical calculations. For instance, in the CH_3 symmetric deformation region the shift of the dimer mode, with respect to that of the monomer, ranges between -4 and 2 cm^{-1} using the MP2/ LanL2DZ+fdp level of theory [18], against of -1 to 3 cm^{-1} in this work using the ωB97X-D/aug-cc-pVTZ-PP level of theory. Similar observations have been found for the trimer, where the shift ranges between -7 to -1 cm^{-1} using the MP2/ LanL2DZ+fdp level of theory [30] and -1 to 8 cm^{-1} using the ωB97X-D/aug-cc-pVTZ-PP one (this work, Table S8). It shows that the bands of dimers and trimers are in close vicinity with those of monomer, what underlies that perturbation induced by CH_3I homo-complexation is weak. Considering that shifts calculated at both levels of theory, that of the present work and the one used by Ito et al. [18,30] are of the same magnitude, it is more accurate to uniquely consider those shifts rather than scaled harmonic frequencies to identify present species. The calculation performed in this study will be used as a support to discriminate between monomers, dimers and trimers observed by FTIR-isolation matrix experiments. Those theoretical vibrational spectra will be studied in fingerprint regions in which they will help to identify species trapped in the matrix.

A typical matrix-isolation infrared (IR) spectra of CH_3I in Ar matrix at 10K and at a mixing ratio of 1/1000 is shown in Fig. S2. The spectrum shows CH_3-stretching (ν_1 and ν_4), deformation (ν_2) and rocking (ν_6) regions centered at 3000, 1250 and 890 cm^{-1}, respectively while the C-I stretching mode is outside the observed spectral region (< 600 cm^{-1}). Additional bands related to traces of water are observed at ~3750 cm^{-1} and 1600 cm^{-1} (not shown). The fundamental bands of the CH_3I monomer are observed at 3054 (not shown), 2965, 1432 (not shown), 1245, 882 and 881(doublet) cm^{-1} for ν_4, ν_1, ν_5, ν_2 and ν_6, respectively. These band positions are consistent with those previously reported for supersonic jet deposition for CH_3I monomer [18,31]. Some additional bands appear on both sides of monomer bands, especially for ν_1, ν_2 and ν_6, which are the most intense bands on the FTIR spectrum (Fig.S2). The observed wavenumbers and the shifts from the monomer are listed in Table 1 and compared with those obtained by calculations. As expected, the set of additional bands are due to the formation of CH_3I clusters. Considering the concentration 1/1000 of CH_3I in Ar matrix, the observation of the monomer bands is the most plausible. However, regarding the calculated and experimental bands the additional ones can be assigned to both HT and HH dimers observed at 2967, 2960, 1248, 1246, 1245, 886 cm^{-1} and 2960, 1244, 886, 881, 878 cm^{-1}, respectively. If the 882-881 doublet is assignable to the monomer, the band at 886 cm^{-1} and that at 879 cm^{-1} present a blue-shift of ≈ +4 and a red-shift of ≈ -3 cm^{-1} with respect to the 882 cm^{-1} one (the most intense of the doublet). Those shifts match $(CH_3I)_2$ HT (+5), and HH (-2). Even if it is more unlikely, the blue-shift could also match with THT_1 and THT_2 trimers. These bands can also be due to Ar sites, what is certainly the case of 882-881 doublet. The 1246-1245 cm^{-1} bands are assigned to two monomer sites, when other observed bands are blue-shifted by ≈ +7 and +3 cm^{-1} and the two latter are red-shifted by ≈ -2 and -6 cm^{-1}. Those shifts allow us to identify unambiguously THT_2 trimer (at 1252 cm^{-1} and tentatively at 1243 and 1239 cm^{-1}), and more tentatively HT dimer and THT_1 trimer (at 1248 cm^{-1}). However, we cannot discard the presence of HH dimer because this latter one presents almost degenerated bands with monomer (see Tables 1 and 2). No clusters larger than $n > 3$ are observed in our experimental conditions. The bands of both monomer and clusters are almost degenerated, which is due to the weakness of CH_3I intermolecular forces (and adopted structures) as previously reported [17]. As a result, the shifts due to the dimer and trimer formation are close to the monomer frequencies. Iodomethane dimers and trimers are more likely formed in the gas phase prior to deposition. The formation of homo-clusters of CH_3I is confirmed by annealing the matrix from 10 to 35K. The FTIR spectra (Fig. S1) clearly show the decrease of the bands of monomer when the IR bands

assigned to dimer or trimer increase. The FTIR spectra (Fig. S3) clearly show the decrease of the monomer bands when those assigned to dimer or trimer increase. This behavior in matrix experiments is explained by the diffusion of CH_3I molecules in the Ar matrix during the annealing. Indeed, Van der Waal radius of iodine atom is large, which results in a limited diffusion of CH_3I within the Ar matrix, moreover on long distance. Thus, we can hypothesis that CH_3I dimers and trimers are formed in the matrix by diffusion of monomers, which are in a close vicinity. This close vicinity may be explained by the fact that cluster of CH_3I are formed in the gaseous phase and partly separated as monomers during the matrix deposition, because of translational kinetic energy relaxation. The further annealing of the close CH_3I molecules is then able to re-form clusters of CH_3I.

In brief, in our experimental conditions we observe CH_3I dimers and trimers formation. These results complete those obtained by Ito et al. [18, 20] in previous studies performed using supersonic jet technic.

Formation of CH_3I-H_2O complexes. The structure and the vibrational spectra of various $(CH_3I)_n$–$(H_2O)_m$ complexes have been calculated at ωB97X-D/aug-cc-pVTZ-PP level of theory for n=1, 2 and m=1, 2, 3. Ito et al. [20] have demonstrated that the B971/LanL2DZ+fdp level of theory reproduces well the MP2/aug-cc-pVTZ level of theory results, while the MP2/LanL2DZ +fdp level of theory underestimates the intermolecular interaction between CH_3I and H_2O for 1:1 complex only. In the present work, the calculations are performed with the ωB97X-D functional with a relativistic effective core potential and an extended valence basis-set for iodine, i.e., aug-cc-pVTZ-PP.

The 1:1, 1:2, 2:1, 2:2 and 1:3 structures were optimized revealing the predicted most stable isomers for each of them as following: 2 isomers for 1:1 and 1:2 structures, 4 isomers for 1:3 structure, 5 isomers for 2:1 structure and 10 isomers for 2:2 structure. The geometry and the standard Gibbs free energies of these isomers are presented in Fig. S4 to S8 with xyz coordinates in Tables S3 to S8 (see SI).

From this theoretical work, valuable information can be retrieved on relative stabilities of each species together with the structure of their vibrational spectra. Indeed, from those results we selected the most accurate spectral regions to discriminate between $(CH_3I)_n$, $(H_2O)_m$ and $(CH_3I)_n$-$(H_2O)_m$ aggregates and complexes.

The 1:1 hetero-dimer (Fig. S4 in SI) presents two stable forms, one pseudo-cyclic, referred as 1:1a, more stable than an unexpected one, 1:1b, which displays a I···O interaction ($\Delta_rG°_{10K}$

= -13.5 kJ mol^{-1}, for 1:1a, against -7.5 kJ mol^{-1}, for 1:1b). Indeed, one could have expected to observe, in 1:1b case, a I···H H-bond interaction, rather than this long distance interaction between iodine and oxygen atoms. Is it so surprising? If one compares, iodine's Pauling electronegativity of 2.66 with that of hydrogen, which is 2.2, it is then plausible to observe a halogen-bond type interaction between iodine and oxygen, this latter presenting a Pauling electronegativity of 3.44. Moreover, the iodomethane dipole moment is oriented toward carbon atom, which leads a partial positive Mulliken's charge for iodine atom in this configuration. It is thus likely that we observe this I···O interaction. The complementary NBO calculations (reported on Fig. S9) show that the distribution of NBO charges within isolated systems (i.e. CH_3I and H_2O monomer) do not greatly differ from those within the 1:1a and 1:1b systems. This indicates that the charge transfer is not the main process while electrostatic interactions are the main forces involved for these systems as we stated. However, the charge transfer influence the geometry of the H-bonds as we have seen on THT_1 and THT_2 structures. Our assumptions are consistent with a recent work [32]. On the vibrational spectra side, one observes a stronger perturbation for 1:1a, with respect to each monomer, H_2O and CH_3I, vibration frequencies, than for 1:1b (see Table S9). Water ν_3 and ν_1 modes are both red-shifted by -28 and -41 cm^{-1}, respectively, while the most obvious shift concerning CH_3I moiety seems to be that of the CH_3 rocking with a blue-shift of 22 cm^{-1}. For 1:1b, water partner presents two almost equivalent free OH bonds, however red-shifted by -11 and -10 cm^{-1}. This result illustrates the iodomethane polarity effect: while there is greater stabilization from the donor-acceptor interaction between the units of the dimer in 1:1b than 1:1a, dimer 1:1a is the lower energy species indicating that electrostatic interactions are mainly responsible for the energy difference between species 1:1a and 1:1b.

For the CH_3I-$(H_2O)_2$ complexes, shown in Fig. S5 (SI), there are three stable structures denoted 1:2a, 1:2b and 1:2c, with $\Delta_rG°_{10K}$ of -45.01, -25.38 and -21.61 kJ mol^{-1}, respectively. If the former one presents a cyclic structure which can be summarized as a water dimer interacting by two H-bond type interactions with CH_3I, the second one displays an almost symmetrical structure with the two water monomers on each side of the CH_3I partner, *i.e.* a kind of double 1:1a (1:1 complex) structure with respect to the ICH iodomethane plane. Regarding the last form, it is the addition of the forms 1:1a and 1:1b (it could be noted that its $\Delta_rG°_{10K}$ is the sum of those of 1:1a and 1:1b species). As a result, on the vibrational spectra of the two first forms, one should observe in 1:2a case, a typical water dimer spectrum, with one proton acceptor, PA, and one proton donor, PD, partner, perturbed by CH_3I, but with the difference

that PA partner also gives its proton to iodine atom, while for 1:2b, one should find a vibrational spectrum close to that of 1:1a. Concerning the last form, 1:2c, it should display a vibrational spectrum really close to those of 1:1a and 1:1b. From Table S10, for 1:2b species, one observes, indeed, comparable shifts with those of 1:1a, for water monomers while CH_3 rocking mode presents more pronounced blue-shifts, by 33 instead of 22 and 22 against 6 cm^{-1}, with respect to 1:1a ones. Another noticeable red-shift is that of CH_3 symmetrical stretching which is -8 cm^{-1}. If we come back to 1:2a species, it is clearly a water dimer spectrum perturbed by CH_3I as illustrated by ν_3 and ν_1 water mode red-shifts. These red-shifts, namely that of -205 cm^{-1} (typical of a ν_1 water dimer PD), coupled to OH···O distance of 1.87 Å (typical of a water dimer) [33], put in evidence that H_2O-H_2O interaction is stronger than interactions of each water monomer with CH_3I partner. As a result it would be difficult to discriminate between 1:2a (in the water region) spectrum and that of the pure water dimer. For 1:2c species, it is easy to see from Tables S9 and S10, that its spectrum will be almost degenerated with those of 1:1a and 1:1b species. As a result it would be quite impossible to discriminate among those three species. Considering this fact, in the remainder of the manuscript, especially in the interpretation of the experimental spectra, if 1:1a and 1:1b are found, this will imply that potentially the 1:2c species is also present.

The CH_3I-$(H_2O)_3$ complex, displayed in Fig. S6 (SI), could be considered as the first step of CH_3I water embedding and could lead to models of CH_3I trapped in water environment as aggregates or Amorphous Solid Water (ASW). We found four different stable structures: (i) 1:3a, the most stable one ($\Delta rG°_{10K}$ = -86.4 kJ mol^{-1}) which is a cyclic water trimer perturbed by CH_3I molecule which should present a vibrational spectrum close to that of cyclic water trimer; (ii) 1:3b, the least stable one ($\Delta rG°_{10K}$ = -37.5 kJ mol^{-1}), which is a kind of spinning top structure with three water molecules interacting independently from each other with a central CH_3I molecule, and should exhibit a spectrum close to that of 1:1a; (iii) 1:3c ($\Delta rG°_{10K}$ = -59.7 kJ mol^{-1}) which displays a kind of "1:1a+1:2a" structure and should therefore share much in common with these two structures; (iv) 1:3d ($\Delta rG°_{10K}$ = -74.8 kJ mol^{-1}) which is a cyclic structure comprising a non-cyclic water trimer bridging both iodine and H atoms of iodomethane. It should be noted that 1:3b and 1:3c should present the strongest CH_3 blue-shifts. One more time, it is obvious that, the greater the number of water molecules involved in self H-bond association, the more stable the hetero-complex or hetero-aggregate is. It comes partly from H-bond interaction efficiency which induces cooperative effects. From the observation of

theoretical harmonic frequencies values (Table S11), it is clear that those signals overlap with those of the other forms.

For the $(CH_3I)_2$-H_2O complexes, shown in Fig. S7 (SI) we count none less than five stable structures denoted, 2:1a to 2:1e, with $\Delta_rG°_{10K}$ lying in a close range of energies (-30.6 to -28.9 kJ mol^{-1}, 2:1b and 2:1c being degenerated), with the exception of 2:1e one, which is a little bit disfavored at -23.8 kJ mol^{-1}). If the three first ones, 2:1a, 2:1b and 2:1c, present quite similar structures, *i.e.* CH_3I dimer interacting with a water monomer (2:1a presenting a subtle double PD, one time PA, character, which gives a small stabilization compared to 2:1b and 2:1c, whose one OH bond remains free), the 2:1d displays water molecule bridging between the two CH_3I molecules while 2:1e presents again the 1:1a moiety in interaction with the other CH_3I partner. Not surprisingly, the most "3D" interacting structures are the most stable. From a vibrational point of view (see Table S12), one can guess that indeed, in the water stretching region, 2:1e presents red-shifts comparable with those of 1:1a but also overlapping with those of 1:2b. Having regard to 2:1a and 2:1d, also in water stretching region, they present comparable red-shifts of -61 cm^{-1} (ν_3), while 2:1a shares its ν_1 red-shift of -54 cm^{-1} with 2:1b and 2:1c. In the CH_3 rocking region, all the species should present the same spectrum, with blue-shifts overlapping with those of the above studied forms.

Concerning $(CH_3I)_2$-$(H_2O)_2$ species, shown in Fig. S8 (SI), we can easily discriminate between two kinds of complexes: those which display a water dimer part, and those which display two separated water molecules. Except for 2:2e ($\Delta_rG°_{10K}$ = -47.9 kJ mol^{-1}), all the former class present the most stable potentials with $\Delta_rG°_{10K}$ ranging from -70.1 (2:2b) to -53.7 (2:2j) kJ mol^{-1}. The latter class displays less stable structures with $\Delta_rG°_{10K}$ ranging from -47.0 (2:2d) to -33.2 (2:2f) kJ mol^{-1}. It could be understood in terms of H-bond type interaction strength. Indeed, in the case of the presence of a water dimer moiety, there is a strong interaction (as illustrated by short OH···H bonds of 1.8-1.9 Å, see Fig S8), due to the quasi-linear interaction between the PD O-H bond and the sp^3 doublet of the PA partner, while in the second category of complexes, interactions between PD and PA are less effective. On the vibrational side, from Table S13, it is obvious that one more time considering OH stretching regions and CH_3 one, if all these isomers coexist, it will induce a spectral congestion. However, some blue-shifts in the ν_2 water bending mode (2:2b, 28 cm^{-1}; 2:2e, 32 cm^{-1}; 2:2g, 35 cm^{-1}; 2:2h, 26 cm^{-1}) could be of some help, even if the 1:2a isomer presents also a blue-shift in this region of 25 cm^{-1}.

The formation of all these species will induce a spectral congestion, so, a careful examination of spectral conditions (namely sample ratii) will be necessary to unambiguously identify all the forms present in argon matrices.

On the experimental vibrational spectra, the two iodomethane spectral regions, *i.e.* ν_2 (bending CH) and ν_6 (rocking mode) are displayed on Fig. 1, while the three water spectral regions, *i.e.* ν_1 (symmetric stretching), ν_2 (bending) and ν_3 (antisymmetric stretching) are presented in Fig. 2 and Fig. S10. We selected those spectral domains because the new bands related to CH_3I-H_2O interaction are well visible on the spectra in these regions. In addition, as discussed above, with the help of theoretical results, we should be able to identify which aggregates and complexes are present in those experimental conditions (with a large excess of water) supposed to mimic atmospheric ones. In Fig.1 and 2 and Fig.S9 (SI) we present a comparison of pure CH_3I spectra with mixed $(CH_3I)_n(H_2O)_m$ ones and of pure water homo-clusters for various spectral regions. New or increasing bands, observed in mixed species spectrum, with respect to those of pure water or iodomethane ones, are marked with a dashed line. The frequencies and assignment are reported in Tables 2 and 3.

It is known that iodomethane is not soluble in water, as a result, it is water self-aggregation which should be favored. However, considering that mixed aggregates and complexes will be trapped in the same matrix cage, we should be able to observe those latter subject to two conditions: they are formed in gas phase prior to sample deposition, and they survive landing on the sample carrier, or they are formed when they land. Indeed the injection mode we used in our experiments is similar to the quenching of a molecular jet when landing on the sample holder. The kinetic energy of translation must then be dissipated which can lead to the dissociation of these complexes. A third way to form those species is to anneal the samples to allow molecules in close neighborhood (few Å to nm) to diffuse through the argon matrix and aggregate. However, iodomethane concentration is so low that homo iodomethane aggregates, by extension hetero complexes with more than one CH_3I molecule, should be formed in gas phase and survive landing at sample carrier.

Considering the large excess of water we used, it seems more appropriate to start by iodomethane vibrational regions ν_2 and ν_6 (Fig. 1 and Table 2). Indeed CH_3I concentration remains 1/1000 with respect to Ar, which limits homo-iodomethane aggregation. Therefore, water addition, if there is aggregation with iodomethane, will lead to less overlapping bands than in the water zone. Between 930 and 850 cm^{-1} (Fig. 1, Table 2), for pure iodomethane

(spectrum (a)), one observes bands centered at 886, 882, 881 and 879 cm^{-1} that are assigned to monomer of CH_3I and CH_3I clusters (dimers and trimers) as presented in the previous part. In the case of mixed iodomethane-water sample (spectrum (b)), one observes the 886 cm^{-1} increase, while 882 and 881 decrease in intensity, and new bands at 909, 903, 899 and 891 cm^{-1} (Table 2). Those latter are blue-shifted by ≈ + 27, +20, +16 and +9 cm^{-1}, with respect to 882 cm^{-1}. These shifts match totally or partially those of the following hetero-complexes and aggregates ($(CH_3I)_n(H_2O)_m$): 1:1a, 1:2a, the 1:3a, 1:3c ones, the whole series 2:1a to 2:1e and the three 2:2f, 2:2g and 2:2h species (Fig. S4 to S8 in SI).

In the ν_2 (bending CH) region (1270-1230 cm^{-1}), one observes, in the case of pure iodomethane, bands at 1248, 1246, 1245, 1243 and 1239 cm^{-1} (Fig. 1, Table 2) that are attributed to CH_3I monomer, dimer and trimer as described in the previous part. In the case of mixed iodomethane-water sample (spectrum (b)), one observes the 1248 cm^{-1} increase, while 1246-1245 decrease in intensity, and new bands at 1257, 1256, 1254 and 1250 cm^{-1} (Table 2). Those latter are blue-shifted by ≈ + 12, 10, 9 and 5 cm^{-1}, with respect to 1245 cm^{-1}. These shifts match totally or partially those of the following hetero-complexes and aggregates ($(CH_3I)_n(H_2O)_m$): 1:1a, 1:2a and 1:2b, the 1:3a and 1:3b, the whole serie 2:1a to 2:1e and the three 2:2c, 2:2d, 2:2f and 2:2g species (Figures S4 to S8). Concerning the species 1:3b, we can already discard its presence because we did not observe blue-shifts of about +44 cm^{-1} in the ν_6 region.

From the analysis of the iodomethane regions (ν_2 and ν_6), we can conveniently discriminate between the first candidates when at least two bands were identified:

$CH_3I.H_2O$ complex: 1:1a

$CH_3I.(H_2O)_2$ complex: 1:2a

$CH_3I.(H_2O)_3$ complex: 1:3a

$(CH_3I)_2.H_2O$ complexes: whole serie 2:1a to 2:1e

$(CH_3I)_2(H_2O)_2$ complexes: 2:2f, 2:2g

Water spectral regions should bring decisive clues in the identification of the different isomers, despite the spectral congestion due to water aggregates.

The H_2O spectral regions (i.e. ν_1, ν_2 and ν_3) are presented in Fig. 2 (ν_1) and in Fig. S10 (ν_2 and ν_3). In the ν_2 region (1770-1510 cm^{-1}), in the case of pure water matrix (Fig. S10 (a)), one observes bands at 1663, 1658, 1637, 1627, 1625, 1620, 1616, 1612, 1611, 1608, 1602, 1599,

1593, 1591, and 1590 cm^{-1}. They are due to water monomer and water clusters [34]. In the case of iodomethane-water mixture (trace (b)), one observes only one new band at 1600 cm^{-1} (Fig. S10), blue-shifted by about ≈ +11 cm^{-1} with respect to the nrm (non rotating monomer) water bending mode at 1589 cm^{-1}. It is a "poor" area because of strong overlapping between water aggregates signals and those of iodomethane-water complexes and aggregates, which should be in minority. As a consequence, the only partial matches found are: 1:3a, which should present theoretically three blue-shifts of ≈ +32, +16 and +10 cm^{-1} (the +32 and +10 cm^{-1} band are certainly overlapped by water aggregates ones), and 2:2a, 2:2e and 2:2j species.

In the ν_1 and water cluster region (3695-3100 cm^{-1}) (Fig. 2(a) and Table 3), one observes bands at 3670, 3662, 3654, 3648, 3647, 3640, 3630, 3628, 3617, 3612, 3574 cm^{-1} (Proton Donor, PD, dimer), 3567, 3564, 3549, 3543, 3528, 3515 cm^{-1} (Trimers), 3445, 3409, 3392, 3373 cm^{-1} (Tetramers), 3332-3325 cm^{-1} (Pentamers), and 3209 cm^{-1} (larger clusters and $2\nu_2$ harmonic mode of H_2O). The first band of interest in the case of mixed samples, is located at 3463 cm^{-1}, *i.e.* between trimers and tetramers. This band is red-shifted with respect to water trimers and blue-shifted with respect to water tetramers, *i.e.* more red-shifted ("perturbed") than a water trimer but less than a water tetramer. This structure is undoubtedly a water trimer perturbed by an iodomethane partner. In Fig. S6, there are only two such structures, 1:3a and 1:3d. Considering that we did not find any evidence of 1:3d presence in the other regions, and that in a large excess of water, this is a cyclic conformation that will be adopted by water, we suggest that this band is assigned to 1:3a. In addition, we have reported a calculated band at 3557 cm^{-1} i.e. redshifted by 322 cm^{-1} for this species (see Table S11) that is not observed on the experimental spectrum. Indeed, because water is overabundant, and considering that IR calculated intensities are indicative in matrix media, this is not surprising not seeing it. The second band of interest is the one centered at 3553 cm^{-1}, red-shifted by ≈ -85 cm^{-1} with respect to ν_1 nrm mode located at 3638 cm^{-1} [34]. This species is located between water dimer Proton Donor (PD) band and those of water trimers. Following the same reasoning, it is thus a water dimer perturbed by an iodomethane partner. In Fig. S5, there is only one structure which matches this water dimer type configuration, this is 1:2a. The mode we observe is the ν_1 stretch of water dimer Proton Acceptor (PA) which bridges to iodine atom. This vibrational assignment is strongly supported by the calculated shift $\Delta\nu$ ≈ -97 cm^{-1} (Table S10), found for this species. However, one has to consider also the presence of 1:3c structure (Fig.S6) which is a "1:2a +1:1a" kind of structure. This last form presents a theoretical red-shift of ≈ -91 cm^{-1} in this region (and also a blue-shift of ≈ +26 cm^{-1} in ν_6 (CH_3I), as mentioned above). The other bands

observed in case of iodomethane-water mixture are centered at 3582, 3603, 3607, 3609 and 3642 cm^{-1}. The four first bands display red-shifts of ≈ -56, -35, -31 and -29 cm^{-1} against a blue-shift of ≈ +4 cm^{-1} for the last one. The only forms which could partially or totally match with those shifts are: 1:1a, 1:3c , the whole serie 2:1a to 2:1e, and 2:2i. As already mentioned, calculated intensities, especially those of the OH modes, ~~they~~ are purely indicative. For instance, in the case of malonaldehyde [35], the OH intensity of the chelated form is calculated to be 0.33 of the most intense OH band among the isomers, but is not observed because of the H-bond strength, which induces a FWHM of thousands of cm^{-1}. As a result, this band is almost flat, and not observed. A similar situation is expected in our case.

In the ν_3 region (3950-3700 cm^{-1}) (Fig. S10 (a) and Table 3)), one observes bands at 3777, 3756, 3753, 3738, 3736, 3731, 3721, 3716, 3711, 3708, 3707, 3703, 3700 and 3695 cm^{-1}. Those bands are mainly due to water monomer and clusters, the non rotating monomer (nrm) and rovibrational transitions [29]. Four new bands are observed in the case of mixed sample, at 3752, 3749, 3720 and 3713 cm^{-1}. If the two highest ones are tentatively assigned to $0_{00} \rightarrow 1_{01}$ water monomer rovibronic transition perturbed by iodomethane proximity, the two lowest ones present red-shift with respect to ν_3 nrm mode of water monomer, located at 3736 cm^{-1} [34] of ≈ -23 and -16 cm^{-1}. Species which present possible matching with those red-shifts are: 1:1a, 1:2b, the whole (1:3) series, 2:1b, 2:1c and 2:1e, 2:2c, 2:2f and 2:2i (Tables S2-S6).

From the combined analysis of the three water regions we can conveniently discriminate between the candidates we have found. Only species presenting at least two distinct bands are considered:

$CH_3I.H_2O$ complex: 1:1a

$CH_3I.(H_2O)_2$ complex: 1:2a

$CH_3I.(H_2O)_3$ complexes: 1:3a,1:3c

$(CH_3I)_2.H_2O$ complexes: whole series from 2:1a to 2:1e

$(CH_3I)_2(H_2O)_2$ complexes: 2:2i

In summary, comparing the candidates identified from both CH_3I and H_2O regions, we can confidently state that we have identified 1:1a, 1:2a and 1:3a, 1:3c species shown on Fig. 3, together with CH_3I monomer, dimers and trimers (Table 2 and 3). It should be noted that they present common bands, this is due to their close structures (see theoretical part). The 1:1a, 1:2a

and 1:3a isomers observed experimentally are consistent with calculated Gibbs free energy given them as the most stable isomers. The structures of dimer or trimer of H_2O perturbed by CH_3I are found in our experimental conditions. This result highlights the preferred formation of hetero aggregates rather than hetero complexes.

Concerning the other possible candidates, either they partially match the observed shifts with no decisive evidence of their presence, or CH_3I being the minority product, 2:1 and 2:2 species are hard to see. The evidence of dimer of CH_3I in our experiments suggests the presence of interaction with water as 2:1 and 2:2 complexes as mentioned above. Indeed, we observed for 2:2i isomer, the only form among all those calculated which present a blue-shift in the ν_1 water region, or 2:1a, 2:1b and 2:1c which could be responsible for the band at 3582 cm^{-1}, while that observed at 3603 cm^{-1} could be assigned to 2:1d and 2:1e species. Because we cannot confirme their presence, we do not include them in Tables 2 and 3.

4. Conclusion

We have investigated the interaction between CH_3I and water molecules using argon cryogenic matrix experiments. The experimental data were supported by theoretical DFT calculations. The experiments were conducted with a large excess of H_2O molecules compared to CH_3I in order to mimic CH_3I environment in the atmosphere. Cryogenic matrices seem pretty accurate in order to describe inter molecular interactions between atmospherically relevant molecules. Even if working at low temperature and pressure does not mimic atmospheric conditions, it brings insights at molecular level. However, working in these conditions allows the study of the ground energy potential of those atmospheric complexes and aggregates. Dimers and trimers of CH_3I are observed despite the high water amount in the initial mixture: this may be explained by the low affinity of CH_3I with water. Monomer of CH_3I perturbing water dimer and trimer are observed rather than hetero complexes that would suggest hetero aggregation process. Finally, considering the concentration of iodomethane used in our experiments and the poor ability of CH_3I to diffuse into the matrix, we state that the aggregates are rather originally formed in the gas phase and not in the matrix cage. The other complexes such as 2:1 and 2:2 cannot be completely excluded but appear as minor species. Thus, the inter molecular behavior between CH_3I and H_2O molecules determined for the first time experimentally and supported by DFT calculation highlights that, in the atmosphere, gaseous iodomethane and water will likely form hetero aggregates of water and iodomethane clusters instead of $(CH_3I)_n$-$(H_2O)_m$ complexes. This result is consistent with recent theoretical studies, which have predicted the

514 incomplete hydration of iodine species [27, 29]. In principle, the abundant low-volatility
515 condensing vapors other than iodine are required in the atmosphere for the growth of iodine
516 clusters to CCN. Our results suggest that the CH_3I would be partially condensed with water on
517 aerosols during the CCN process rather than serves as CCN it-self. The Henry constant value
518 (H^{CP} (at 298 K) = 2-3.5 10^{-3} $mol.m^{-3}.Pa^{-1}$ [36]) predicts that CH_3I will remain in the gaseous
519 phase and thus, will be subject to the oxidative photolysis to form in term iodine oxide particles
520 (IOPs) [37]. The atmospheric gas-to-particle conversion mechanism requires initial clustering
521 steps, which are driven by I_xO_y in both dry and humid conditions. However, the IR and UV
522 photolysis of hetero aggregates in gaseous phase has not been considered until now. In the
523 future, the photochemical behavior of such CH_3I-water aggregates will be investigated. Finally,
524 in the context of the NNP's severe accident, our work is contributing to better understand the
525 fate of nuclear species in the atmosphere and thus, the radionuclide dispersion.
526

527 **Author statement**

528 Sophie Sobanska: Oversight and leadership responsibility for the research activity planning and
529 execution, acquisition of the financial support for the project leading to this publication, writing,
530 reviewing and editing the paper.
531 Hanaa Houjeij: Perfoming the experiments and theoretical calculations
532 Stephane Coussan: Participating to the interpretation of the experimental and theoretical results
533 and to the manuscript writing and reviewing.
534 Christian Aupetit: Providing experimental services
535 Sonia Taamali: Providing training and support for theoretical calculations
536 Florent Louis: Providing a part of theoretical discussion and of computational section writing.
537 Laurent Cantrel: Participating to the acquisition of the financial support.
538 Anne Cécile Gregoire: Acquisition of the financial support, reviewing of the paper.
539 Joëlle Mascetti: Formulation and evolution of overarching research goal and aims, performing
540 the experiments.

541 **Declaration of competing interest**

542 No potential conflict of interest is reported by the authors

543

544

Acknowledgments

Authors acknowledges funding from Region Nouvelle Aquitaine and IRSN for the financial support through the project SPECAERO n° 2017-1R10108-00013012. Computer time for part of the theoretical calculations was kindly provided by the Centre de Ressources Informatiques (CRI) of the University of Lille and the Centre Régional Informatique et d'Applications Numériques de Normandie (CRIANN). S. Sobanska, J. Mascetti and S. Coussan thank GDR-EMIE (GDR CNRS 3533) for the financial support of a joint project.

REFERENCES

[1] J. Didier, A. Bentaïb, H. Bonneville, G. Cénérino, B. Clément, F. Corenwinder, M. Cranga, G. Ducros, F. Fichot, D. Jacquemain, et al. Nuclear Power Reactor Core Melt Accidents; EDP Sciences : Science and Technology Series, France, 2015.

[2] A. Karhu, Gas Phase Chemistry and Removal of CH_3I during a Severe Accident; Report: NKS-25, ISBN 87-7893-076-6. Corpus ID: 59022982. Danka Services International, DSI.; Denmark, 2001. http://www.nks.org/en/documents_test/view_document.htm?id=111010111119718

[3] H. Bruchertseifen, R. Cripps, S. Güntay, B. Jäckel, Experiments on the Retention of the Fission Product Iodine in Nuclear Reactor Accidents [CH--0401]. Report NIS/IAEA, Reference Number 36002863 Gschwend, B. [Ed.]. Switzerland, 2004.

[4] G.Steinhauser, A.Brandl, T. E. Johnson, Sci. Total Environ. 470–471 (2014) 800–817. https://doi.org/10.1016/j.scitotenv.2013.10.029.

[5] S. Dickinson, A. Auvinen, Y. Ammar, L. Bosland, B. Clément, F. Funke, G. Glowa, T. Kärkelä, D.A. Powers, S. Tietze, S.; et al., , Ann. Nucl. Energy 74 (2014) 200–207. https://doi.org/10.1016/j.heliyon.2018.e00553

[6] S. Guentay, R.C. Cripps, B. Jäckel, H. Bruchertseifer, Chimia 59 (2005) 957–965. https://doi.org/10.2533/000942905777675453

[7] L.S. Lebel, R.S. Dickson, G.A. Glowa, J. Environ. Radioact. 151 (2016) 82–93. https://doi.org/10.1016/j.jenvrad.2015.06.001

[8] M. Chebbi, B. Azambre, C. Volkringer, T. Loiseau, Microporous Mesoporous Mater. 259 (2018) 244–254. https://doi.org/10.1016/j.micromeso.2017.10.018

[9] L. Bosland, S. Dickinson, G. Glowa, L.E. Herranz, H.C. Kim, D.A. Powers, M. Salay, S. Tietze, Ann. Nucl. Energy 74 (2014) 184–199. https://doi.org/10.1016/j.anucene.2014.07.016

[10] L.J. Carpenter, Chem. Rev. 103 (2003) 4953–4962. https://doi.org/10.1021/cr0206465

[11] A. Saiz-lopez, J.M.C Plane, A.R. Baker, L.J. Carpenter, R. Von Glasow, C.G. Juan, G. Mcfiggans, R.W. Saunders, Chem. Rev. 112 (2012) 1773–1804. https://doi.org/10.1021/cr200029u

[12] W.R. Simpson, S.S.Brown, A. Saiz-Lopez, J.A. Thornton, R. Von Glasow, Chem. Rev. 115 (2015) 4035–4062. https://doi.org/10.1021/cr5006638

[13] R.M. Moore, C.E. Geen, V.K. Tait, Chemosphere 30 (1995) 1183–1191. https://doi.org/10.1016/0045-6535(95)00009-W

[14] S. Elliottl, F. Sherwood, F., Geophys. Res. Lett. 20 (1993) 1043–1046. https://doi.org/10.1029/93GL01081

[15] L. Feketeová, P. Bertier, T. Salbaing, T. Azuma, F. Calvo, B. Farizon, M. Farizon, T.D. Märk, Proc. Natl. Acad. Sci. U. S. A. 116 (2019) 22540–22544.

https://doi.org/10.1073/pnas.1911136116
[16] A. Habartová, A. Obisesan, B. Minofar, M. Roeselová, Theor. Chem. Acc. 133 (2014) 1–15. https://doi.org/10.1007/s00214-014-1455-z
[17] P. Ramasami, T.A. Ford, J. Mol. Struct. 1126 (2016) 2–10. https://doi.org/10.1007/s00894-019-3927-5
[18] F. Ito, T. Nakanaga, Y. Futami, S. Kudoh, M. Takayanagi, M. Nakata, Chem. Phys. Lett. 343 (2001) 185–191. https://doi.org/10.1016/S0009-2614(01)00688-1
[19] Y. Futami, S. Kudoh, F. Ito, T. Nakanaga, M. Nakata, J. Mol. Struct. 690 (2004) 9–16. https://doi.org/10.1016/j.molstruc.2003.10.037
[20] F. Ito, J. Mol. Struct. 1035 (2013) 54–60. https://doi.org/10.1016/j.molstruc.2012.09.027
[21] Z. Guennoun, C. Aupetit, J. Mascetti, Phys. Chem. Chem. Phys. 13 (2011) 7340–7347. https://doi.org/10.1039/C0CP01756F
[22] Z. Guennoun, C. Aupetit, J. Mascetti, J. Phys. Chem. A 115 (2011) 1844–1852. https://doi.org/10.1021/jp108713n
[23] V. Deguin, J. Mascetti, A. Simon, N. Ben Amor, C. Aupetit, S. Latournerie, J. Noble, J. Phys. Chem. A 122 (2018) 529–542. https://doi.org/10.1021/acs.jpca.7b09681
[24] M.J. Frisch, G. Trucks, H.B. Schlegel, G.E. Scuseria, M.A. Robb, J. Cheeseman, G. Scalmani, V. Barone, B. Mennucci, G.A. Petersson, et al. Gaussian 09, Revision A.1., Gaussian, Inc.: Wallingford, CT. 2009.
[25] J. Da Chai, M. Head-Gordon, Phys. Chem. Chem. Phys. 10 (2008) 6615–6620. https://doi.org/10.1039/B810189B
[26] K.A. Peterson, B.C. Shepler, D. Figgen, H. Stoll, J. Phys. Chem. A 110 (2006) 13877–13883. https://doi.org/10.1021/jp065887l
[27] A. Villard, S. Khanniche, C. Fortin, L. Cantrel, I. Černušák, F. Louis, Int. J. Quantum Chem. 119 (2019) 1–11. https://doi.org/10.1002/qua.25792
[28] K.K. Irikura. THERMO.PL, National Institute of Standards and Technology, Gaithersburg, MD, USA 2000.
[29] S. Taamalli, D. Khiri, S. Suliman, S. Khanniche, I. Černušák, L. Cantrel, M. Ribaucour, F. Louis, ACS Earth Space Chem. 4 (2020) 92-100. https://doi.org/10.1021/acsearthspacechem.9b00257
[30] F. Ito, T. Nakanaga, Y. Futami, M. Nakata, Chem. Phys. 286 (2003) 337–345. https://doi.org/10.1016/S0301-0104(02)00919-9
[31] A.J. Barnes, M. L.Evans, H.E. Hallam, J. Chem. Soc., Faraday Trans. 2, 69 (1973) 738–749. https://doi.org/10.1039/F29736900738
[32] J.M. Herbert and K. Carter-Fenk, J Phys Chem A. 125 (2021) 1243-1256. https://doi.org/10.1021/acs.jpca.0c11356.
[33] S. Coussan, P. Roubin, J.P. Perchard, Chem. Phys. 324 (2006) 527–540. https://doi.org/10.1016/j.chemphys.2005.11.017
[34] J. P. Perchard. Chem. Phys. 273 (2001), 217–213. https://doi.org/10.1016/S0301-0104(01)00496-7
[35] A.Trivella, T. N.Wassermann; C. Manca Tanner, N. O. B. Lüttschwager, S. Coussan, J. of Phys. Chem. A 122, (2018) 2376-2393. https://doi.org/10.1021/acs.jpca.7b11980
[36] R. Sander, Atmos. Chem. Phys. 15, (2015) 4399–4981. https://doi.org/10.5194/acp-15-4399-2015
[37] J.C. Gomez Martin, T.R. Lewis, M.A. Blitz, J.M.C. Plane, M. Kumar, J.S. Francisco, A. Saiz-Lopez, Nature com. 11 (2020) 4521-4521. https://doi.org/10.1038/s41467-020-18252-8

638 **Figure captions:**

639 Fig. 1: IR spectra in ν_2 [bending CH), ν_6 (rocking CH_3) regions of pure iodomethane matrix
640 (trace (a)) (CH_3I/Ar = 1/1000), recorded at 10 K, and of mixed CH_3I/H_2O/Ar = 1/25/1500,
641 recorded at 10 K (trace (b)).

642 Fig. 2: IR spectra in ν_1 (antisymmetric stretching) region of pure water cluster matrix (trace (a))
643 (H_2O/Ar = 7/1000), recorded at 4 K, and of mixed CH_3I/H_2O/Ar = 1/25/1500, recorded at 10 K
644 (trace (b)).

645 Fig. 3: Calculated structures of the unambiguously identified $(CH_3I)_n$-$(H_2O)_m$ isomers at the
646 ωB97X-D/ aug-cc-pVTZ-PP level of theory observed experimentally

647 **Table captions:**

648 Table 1: Table 1: Experimental IR band positions for ν_1, ν_2 and ν_6 (in cm^{-1}) for CH_3I (1000
649 ppm) in Ar matrix, observed and calculated shift from the monomer and tentative assignment
650 (in bold the most intense IR bands) – Experimental IR band positions for ν_1, ν_2 and ν_6 (in cm^{-1})
651 for CH_3I (1000 ppm) in Ar matrix from (18) and (31) and CH_3I in gas phase from (31).

652 Table 2: Experimental IR band positions for ν_1, ν_2, and ν_6 (in cm^{-1}) in CH_3I spectral range for
653 mixed CH_3I/H_2O/Ar = 1/25/1500, recorded at 10 K, calculated spectral shifts ($\Delta\nu$) to
654 experimental spectrum of CH_3I monomer and tentative assignment.

655 Table 3: Experimental IR band positions for ν_1, and ν_3 (in cm^{-1}) in H_2O spectral range for
656 reference spectra of monomer and dimer, mixed CH_3I/H_2O/Ar = 1/25/1500, recorded at 10 K,
657 for H_2O (4:1000) at 4K, calculated spectral shift ($\Delta\nu$) to experimental spectrum for H_2O
658 monomer and tentative assignment.

659

660

661

Tables

Table 1: Experimental IR band positions for ν_1, ν_2 and ν_6 (in cm^{-1}) for CH_3I (1000 ppm) in Ar matrix, observed and calculated shift from the monomer and tentative assignment (in bold the most intense IR bands) – Experimental IR band positions for ν_1, ν_2 and ν_6 (in cm^{-1}) for CH_3I (1000 ppm) in Ar matrix from [18] and [31] and CH_3I in gas phase from (31).

Vibrational modes		**ν experimental cm^{-1}**	**$\Delta\nu$ from monomer**		**ν cm^{-1} [18]**	**ν cm^{-1} [31]**	**$\nu_{gas\ phase}$ cm^{-1} [31]**	**tentative assignment**
			obs	**cal**				
ν_1	CH_3 stretch	2976	11	-				-
		2967	2	2				dimer HT
		2965	0	0	2965	2965	2953	monomer / trimer THT_1
		2960	-5	2 / -2 /-4				dimer HT / dimer HH / trimer THT_1
ν_2	Sym CH_3 deformation	1248	3	3				dimer HT / trimer THT_1
		1246	1	0				dimer HT / trimer THT_1
		1245	0	0	1245	1245	1251	monomer / dimer HT
		1244	-1	-1				dimer HH
		1243	-2	-2				trimer THT_1
		1240	-5	-				-
ν_6	CH_3 rocking	886	4	5 / 3				dimer HT / dimer HH / trimer THT_1
		882	0	0	882		882	monomer / dimer HH
		881	-1	-1	880	880		monomer/ dimer HH
		878	-4	-2				dimer HH

669 Table 2: Experimental IR band positions for ν_1, ν_2, and ν_6 (in cm^{-1}) in CH_3I spectral range for
670 mixed $CH_3I/H_2O/Ar$ = 1/25/1500, recorded at 10 K, calculated spectral shifts ($\Delta\nu$) to
671 experimental spectrum of CH_3I monomer and tentative assignments.

Vibrational Mode	**CH_3I monomer**	**CH_3I-H_2O**	**$\Delta\nu$**	**tentative assignments**
ν_1 CH_3I		2976	11	CH_3I
		2968	3	dimer HT
	2965	2965	0	monomer / trimer THT_1
		2961	-4	dimer HT / dimer HH / trimer THT_1
		2925		n.c.
		2868		n.c.
		2855		n.c.
		2846		n.c.
		2825		n.c.
		2819		n.c.
ν_2 CH_3I		**1257**	**12**	**CH_3I-$3H_2O$ (1 :3a)**
		1256	**11**	**CH_3I-$3H_2O$ (1 :3a)**
		1254	**9**	**see text**
		1250	**5**	**CH_3I-$2H_2O$ (1 :2a)**
		1248	**3**	dimer HT / trimer THT_1 / **CH_3I-H_2O (1:1a)**
		1246	1	dimer HT / trimer THT_1
	1245	1245	0	monomer / dimer HT /
		1243	-2	dimer HH/ trimer THT_1
		1240	-5	CH_3I
ν_6 CH_3I		**909**	**27**	**CH_3I-$2H_2O$ (1:2a) / CH_3I-$3H_2O$ (1:3c)**
		903	**21**	**CH_3I-H_2O (1 :1a)**
		899	**17**	**CH_3I-$2H_2O$ (1:2a) / CH_3I-$3H_2O$ (1:3a)**
		896	**14**	**CH_3I-$3H_2O$ (1:3a)**
		891	**11**	**CH_3I-H_2O (1 :1a)**
		888	**6**	**see text**
		886	**4**	dimer HT / dimer HH / trimer THT_1 / **CH_3I-$3H_2O$ (1:3a)**
	882	882	0	monomer / dimer HH
	881	881	-1	monomer/ dimer HH
		879	-2	dimer HH

672

673

Table 3: Experimental IR band positions for ν_1, and ν_3 (in cm^{-1}) in H_2O spectral range for reference spectra of monomer and dimer, mixed $CH_3I/H_2O/Ar$ = 1/25/1500, recorded at 10 K, for H_2O (4:1000) at 4K, calculated spectral shifts ($\Delta\nu$) to experimental spectrum for H_2O monomer and tentative assignments.

H_2O monomer and dimer[29]	**H_2O 4:1000**	**CH_3I-H_2O**	**$\Delta\nu$**	**tentative assignements**
3776	3777	3777		H_2O rovibrationnal band ν_3
3757	3756	3756		H_2O rovibrationnal band ν_3
	3753	3753		H_2O rovibrationnal band ν_3
		3752	**16**	**see text**
		3749	**13**	**see text**
3739				H_2O rovibrationnal band ν_3
3738	3738	3738		H_2O dimer PA
3736	3736	3736		H_2O ν_3 [nrm)
	3731	3731		H_2O rovibrationnal band ν_3
3725	3721	3721		H_2O rovibrationnal band ν_3
		3720	**-16**	**CH_3I-$3H_2O$ [1 :3c)**
3716	3716	3716		H_2O dimer PD
3711	3711	3711		H_2O rovibrationnal band ν_3
		3713	**-23**	**CH_3I-H_2O [1:1a) / CH_3I-$3H_2O$ [1:3c)**
3708	3708			H_2O dimer PD
3670	3670	3670		H_2O dimer PD / H_20 rovibrationnal band ν_1
	3662	3662		H_2O dimer PD
3654	3654	3654		H_2O dimer PD / H_20 rovibrationnal band ν_1
	3648	3648		H_2O dimer PD
	3647	3647		H_2O dimer PD
		3642	**4**	**see text**
	3640	3640		H_2O dimer PD
3638	3638	3638		H_2O ν_1 [nrm)
3633	3633	3633		H_2O dimer PA
	3630	3630		H_2O dimer PD
	3628	3628		H_2O dimer PD
3623				H_2O rovibrationnal band ν_1
	3617	3617		H_2O dimer PD
	3612	3612		H_2O dimer PD
		3609	**-29**	**CH_3I-H_2O [1 :1a)**
3607	3607	**3607**	-31	H_2O rovibrationnal band ν_1 **/ see text**
		3603	**-35**	**see text**
		3582	**-56**	**see text**
3574	3576	3574		H_2O dimer PD
	3567	3567		H_2O trimer
	3564	3564		H_2O trimer
		3553	**-85**	**CH_3I-$2H_2O$ [1:2a) / CH_3I-$3H_2O$ [1:3c)**
	3549	3549		H_2O trimer
	3543	3543		H_2O trimer
	3528	3528		H_2O trimer
	3515	3515		H_2O trimer

		3463	**-175**	**CH_3I-3H_2O [1 :3a)**
	3445	3445		H_2O tetramer
	3402	3402		H_2O tetramer
	3392	3392		H_2O tetramer
	3373	3373		H_2O tetramer
	3332	3332		H_2O pentamer
	3325	3325		H_2O pentamer
	3209	3209		H_2O High polymer / $2\nu_2$ harmonic

678

679

680

Figures

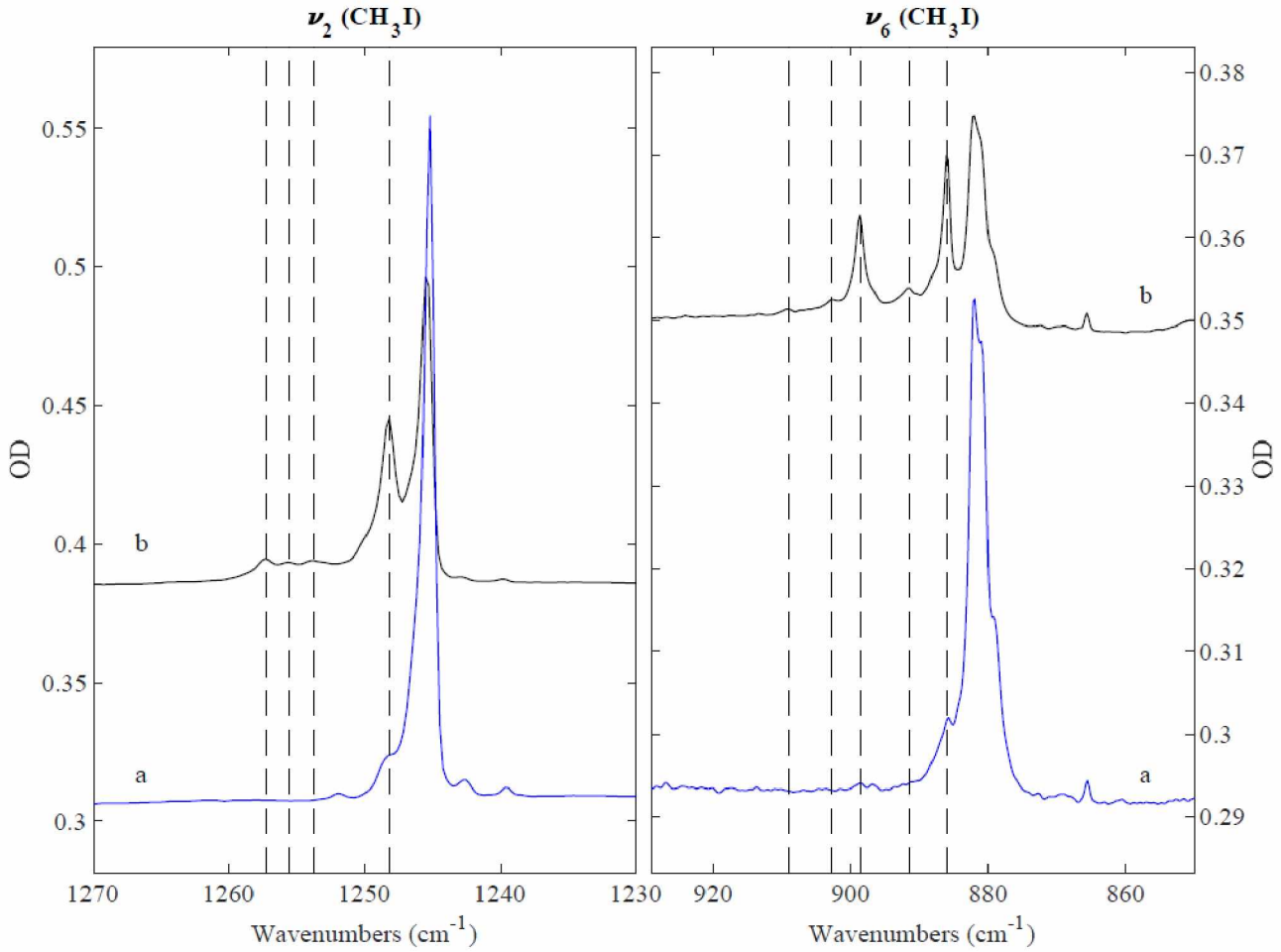

Fig. 1 : IR spectra in ν_2 (bending CH), ν_6 (rocking CH_3) regions of pure iodomethane matrix (trace [a]) (CH_3I/Ar = 1/1000), recorded at 10 K, and of mixed CH_3I/H_2O/Ar = 1/25/1500, recorded at 10 K (trace (b)).

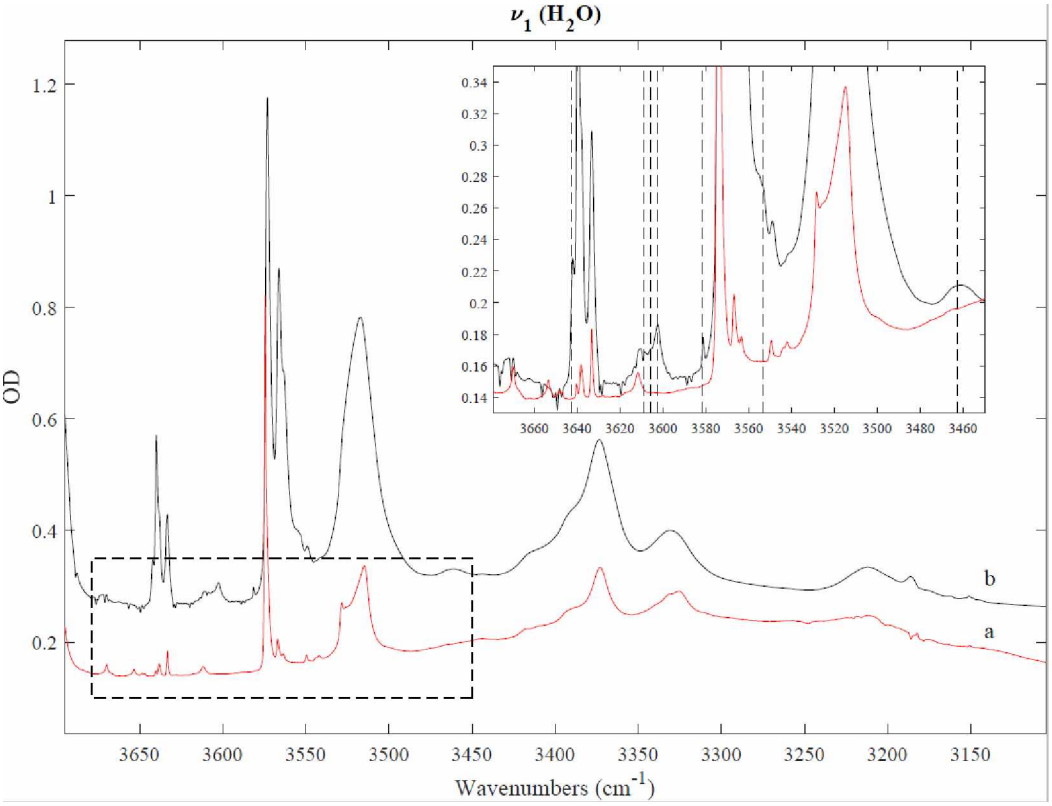

689

690 Fig. 2: IR spectra in the ν_1 (antisymmetric stretching) regions of pure water cluster matrix [trace
691 (a)) (H_2O/Ar = 7/1000), recorded at 4 K, and of mixed CH_3I/H_2O/Ar = 1/25/1500, recorded at
692 10 K (trace (b)).

693

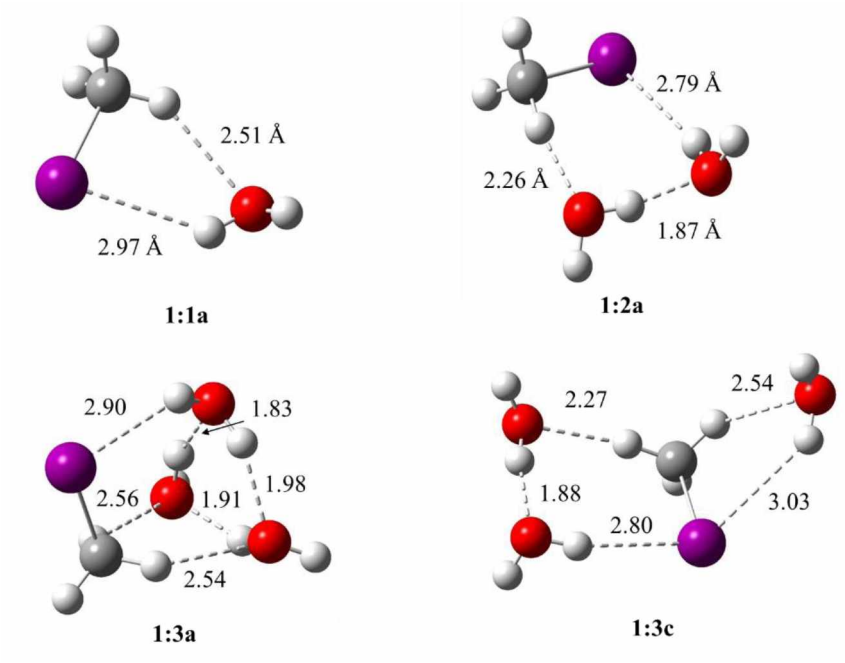

694

695 Fig. 3: Calculated structures of the unambiguously identified $(CH_3I)_n$-$(H_2O)_m$ isomers at the
696 ωB97X-D/ aug-cc-pVTZ-PP level of theory observed experimentally

697

698

699

700

701

Infrared matrix-isolation and theoretical studies of interactions between CH_3I and water

Sophie Sobanska[1]*, Hanaa Houjeij[1,4], Stéphane Coussan[2], Christian Aupetit[1], Sonia Taamalli[3], Florent Louis[3], Laurent Cantrel[4], Anne Cécile Gregoire[4], Joëlle Mascetti[1]

1- Institut des Sciences Moléculaires, Université de Bordeaux, UMR5255 CNRS, 33405 Talence cedex, France

2- CNRS, Aix-Marseille Univ, PIIM, Marseille13397, France

3- Physico-Chimie des Processus de Combustion et de l'Atmosphère, Université de Lille, UMR8522 CNRS, 59000 Lille, France

4- Institut de Radioprotection et de Sûreté Nucléaire, IRSN/PSN-RES, Cadarache, 13115 St Paul Lez Durance, France

*corresponding author: sophie.sobanska@u-bordeaux.fr

Highlights:

- Microhydration of iodomethane is explored by matrix isolation infrared spectroscopy
- Microhydration with a large excess of water is investigated
- Hetero-aggregates between CH_3I and H_2O are formed with dimers and trimers of CH_3I
- Interaction between CH_3I and H_2O is not favored in the atmosphere

Graphical Abstract

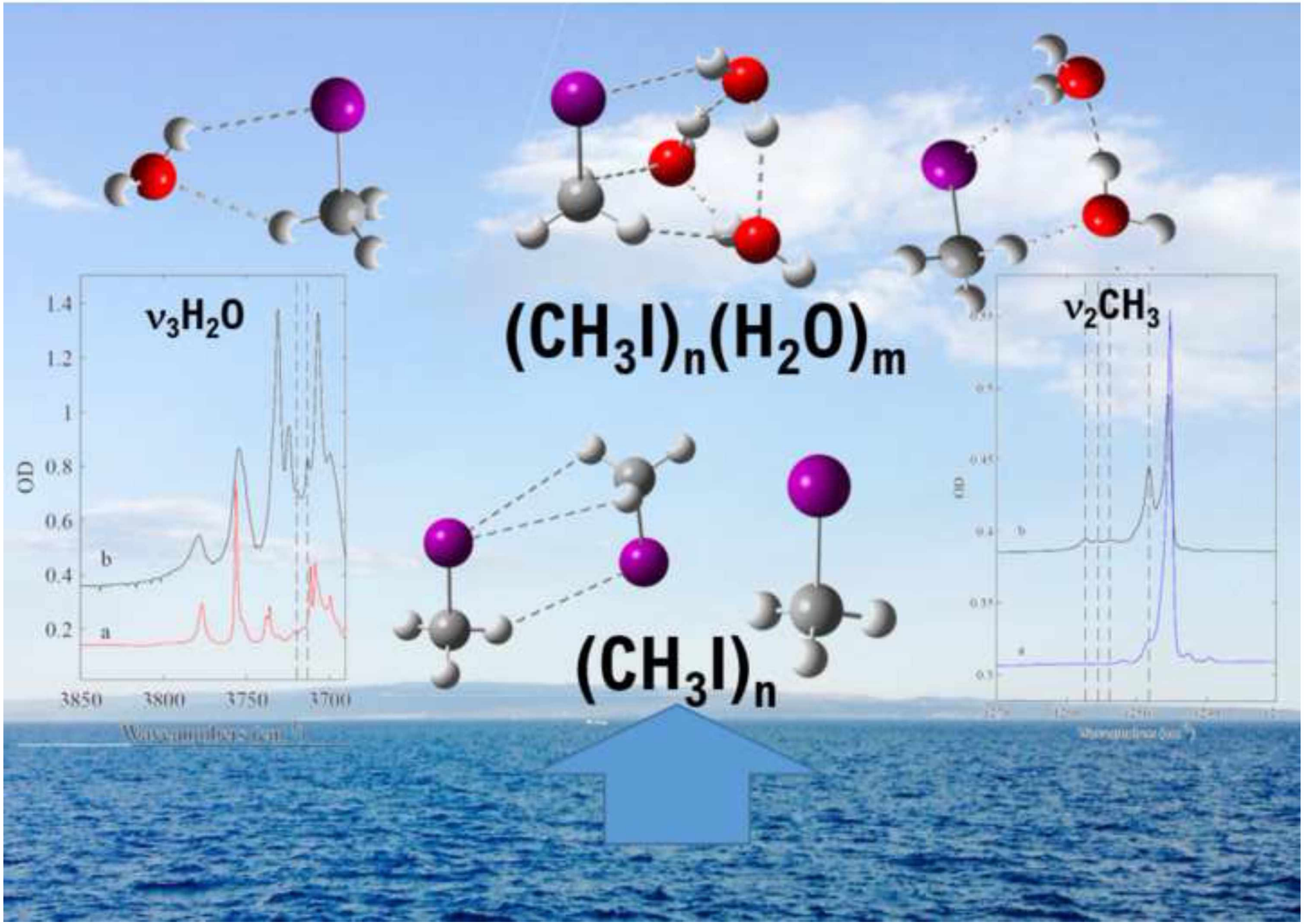

Infrared matrix-isolation and theoretical studies of interactions between CH_3I and water

Sophie Sobanska[1]*, Hanaa Houjeij[1,4], Stéphane Coussan[2], Christian Aupetit[1], Sonia Taamalli[3], Florent Louis[3], Laurent Cantrel[4], Anne Cécile Gregoire[4], Joëlle Mascetti[1]

1- Institut des Sciences Moléculaires, Université de Bordeaux, UMR5255 CNRS, 33405 Talence cedex, France

2- Physique des interactions ioniques et moléculaires, UMR7345 CNRS, Aix-Marseille Université, 13013 Marseille, France

3- Physico-Chimie des Processus de Combustion et de l'Atmosphère, Université de Lille, UMR8522 CNRS, 59000 Lille, France

4- Institut de Radioprotection et de Sûreté Nucléaire, IRSN/PSN-RES, Cadarache, 13115 St Paul Lez Durance, France

*corresponding author: sophie.sobanska@u-bordeaux.fr

Supporting information

Figure list:

Fig. S8: ωB97X-D/aug-cc-pVTZ-PP-predicted geometry (distances in Å) and Gibbs free energy (ΔG in kJ mol^{-1}) of $(CH_3I)_2.(H_2O)_2$ isomers.

Fig. S9: Distribution of NBO charges calculated at ωB97X-D/aug-cc-pVTZ level of theory for CH_3I, H_2O monomers and 1:1a and 1:1b complexes.

Fig. S10: IR spectra in the ν_3 (symmetric stretching) and ν_2 (bending mode) regions of pure water cluster in matrix (trace (a)) (H_2O/Ar = 7/1000), recorded at 4 K, and of mixed CH_3I/H_2O/Ar = 1/25/1500, recorded at 10 K (trace (b) new bands are marked with dashed lines).

Table list:

Table S1. Optimized Cartesian Coordinates of $(H_2O)n$ at the ωB97X-D/aug–cc–pVTZ level of theory
Table S2. Optimized Cartesian Coordinates of $(CH_3I)n$ at the ωB97X-D/aug–cc–pVTZ level of theory
Table S3. Optimized Cartesian Coordinates of $CH_3I.H_2O$ at the ωB97X-D/aug–cc–pVTZ level of theory
Table S4. Optimized Cartesian Coordinates of $CH_3I.(H_2O)_2$ at the ωB97X-D/aug–cc–pVTZ level of theory
Table S5. Optimized Cartesian Coordinates of $CH_3I.\ (H_2O)_3$ at the ωB97X-D/aug–cc–pVTZ Level of Theory
Table S6. Optimized Cartesian Coordinates of $(CH_3I)_2.H_2O$ at the ωB97X-D/aug–cc–pVTZ level of theory
Table S7. Optimized Cartesian Coordinates of $(CH_3I)_2.(H_2O)_2$ at the ωB97X-D/aug–cc–pVTZ level of theory
Table S8. Calculated wavenumbers (cm^{-1}) and intensities (I in km/mol) of CH_3I monomer, HH and HT dimers and THT_1 and THT_2 trimers. The IR bands are predicted at the ωB97X-D/aug-cc-pVTZ-PP level of theory. The frequency shifts are calculated with respect to the monomer position ($\Delta\nu = \nu - \nu_{monomer}$).

Table S9. Calculated wavenumbers (cm^{-1}) and intensities (I in km/mol) of $CH_3I.H_2O$ complexes compared to the calculated wavenumber (cm^{-1}) and intensities (I) of CH_3I monomer and H_2O monomer and dimer. The IR bands are predicted at the ωB97X-D/aug-cc-pVTZ-PP level oft. The frequency shifts are calculated with respect to the monomer position ($\Delta\nu = \nu - \nu_{monomer}$).

Table S10. Calculated wavenumbers (cm^{-1}) and intensities (I in km/mol) of $CH_3I.(H_2O)_2$ complexes compared to the calculated wavenumber (cm^{-1}) and intensities (I) of CH_3I monomer and H_2O monomer and dimer. The IR bands are predicted at the ωB97X-D/aug-cc-pVTZ-PP level of theory. The frequency shifts are calculated with respect to the monomer position ($\Delta\nu = \nu - \nu_{monomer}$).

Table S11. Calculated wavenumbers (cm^{-1}) and intensities (I in km/mol) of $CH_3I.(H_2O)_3$ complexes compared to the calculated wavenumber (cm^{-1}) and intensities (I) of CH_3I monomer and H_2O monomer and dimer. The IR bands are predicted at the ωB97X-D/aug-cc-pVTZ-PP level of theory. The frequency shifts are calculated with respect to the monomer position ($\Delta\nu = \nu - \nu_{monomer}$).

Table S12. Calculated wavenumbers (cm^{-1}) and intensities (I in km/mol) of $(CH_3I)_2.(H_2O)$ complexes compared to the calculated wavenumber (cm^{-1}) and intensities (I) of CH_3I monomer and H_2O monomer and dimer. The IR bands are predicted at the ωB97X-D/aug-cc-pVTZ-PP level of theory. The frequency shifts are calculated with respect to the monomer position ($\Delta\nu = \nu - \nu_{monomer}$).

Table S13. Calculated wavenumbers (cm^{-1}) and intensities (I in km/mol) of $(CH_3I)_2.(H_2O)_2$ complexes compared to the calculated wavenumber (cm^{-1}) and intensities (I) of CH_3I monomer and H_2O monomer and dimer. The IR bands are predicted at the ωB97X-D/aug-cc-pVTZ-PP level of theory. The frequency shifts are calculated with respect to the monomer position ($\Delta\nu = \nu - \nu_{monomer}$).

89

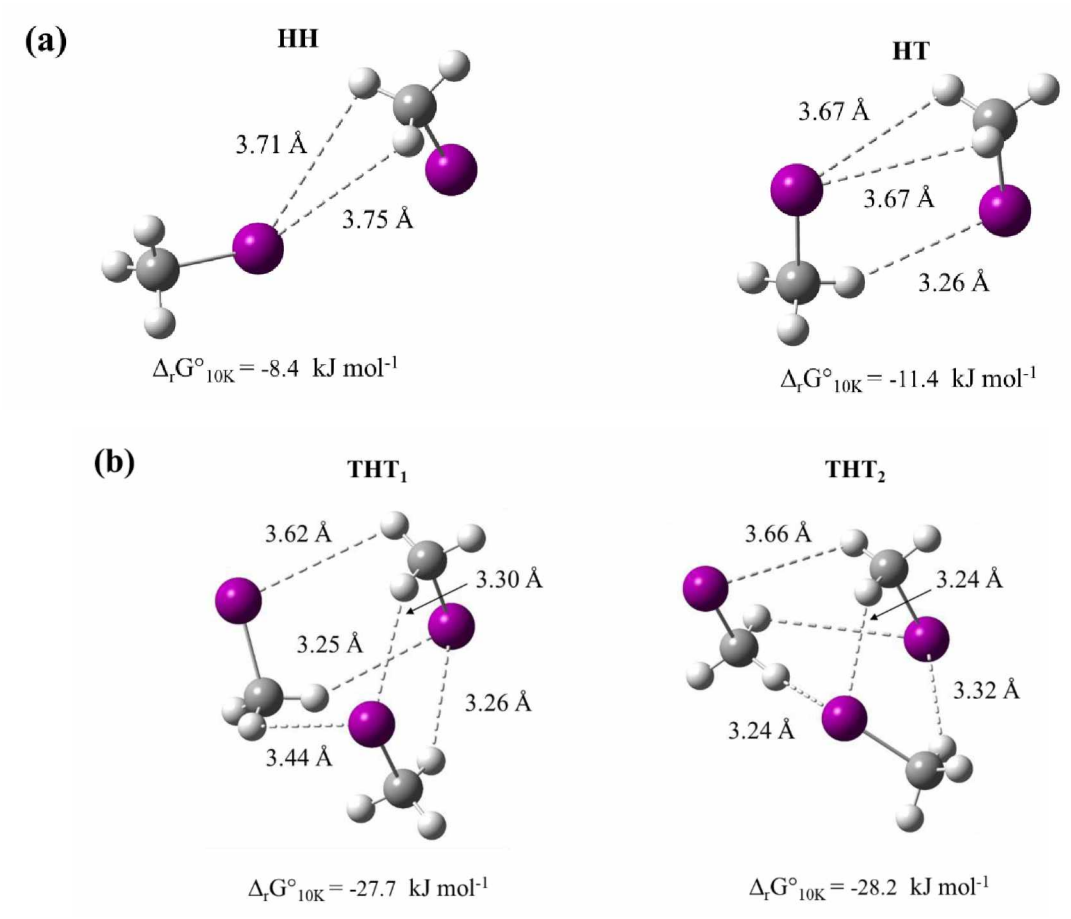

Fig. S1: ωB97X-D/ aug-cc-pVTZ-PP-predicted geometries (distances in Å) and Gibbs free energies (ΔG in kJ/mol) of CH_3I dimers (a) and trimers (b).

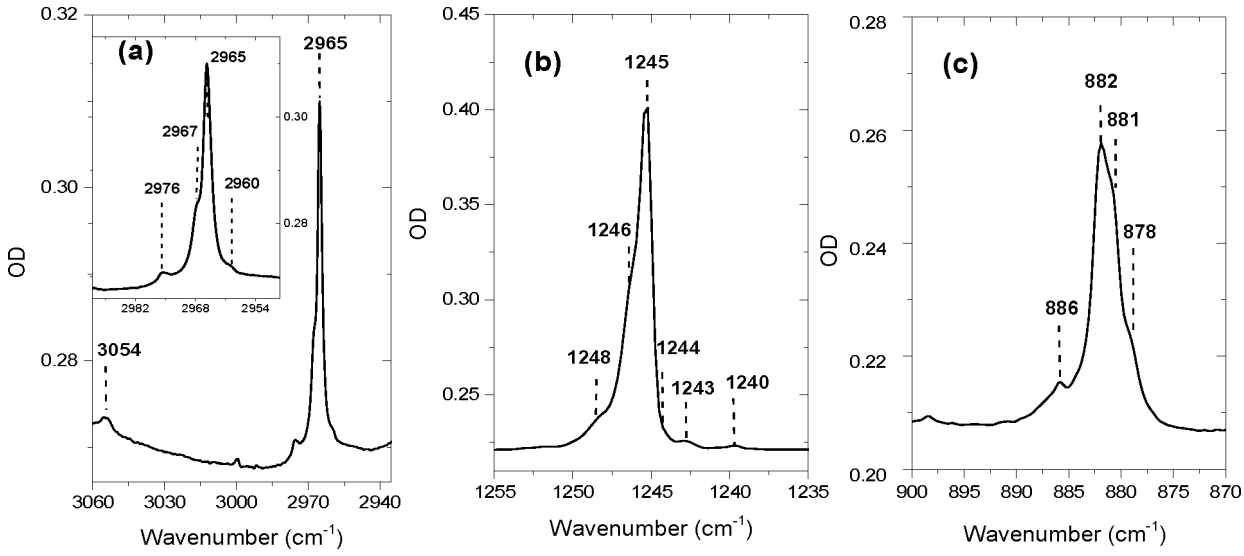

Fig. S2: IR spectra of CH_3I/Ar sample at 10 K in the 3100-2750 cm^{-1} and 1350-750 cm^{-1} spectral range corresponding to (a) the CH_3 stretching (ν_1, (b) CH_3 deformation (ν_2) and (c) rocking (ν_6) regions, respectively.

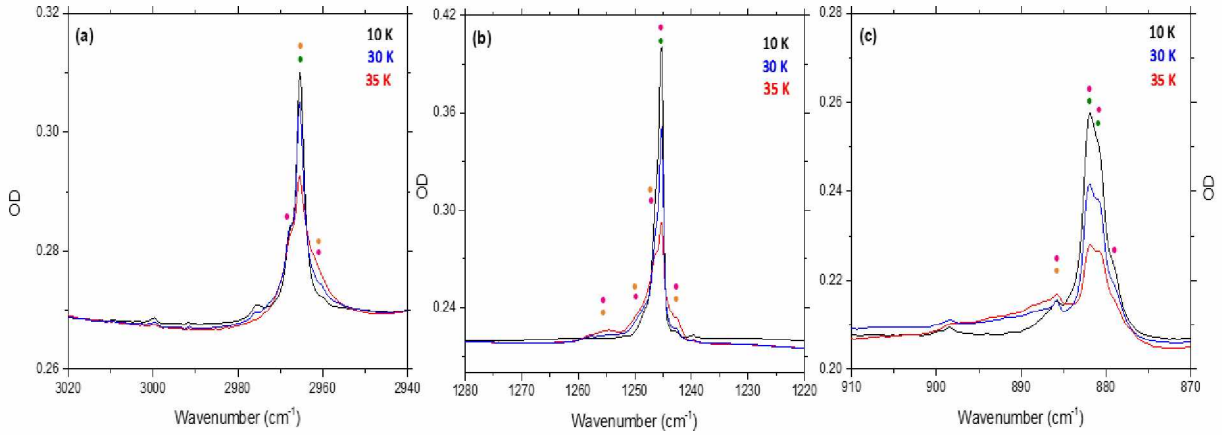

Fig. S3: IR spectra of the annealing of CH_3I/Ar sample until 35 K in the spectral range (a) 3020-2940 cm^{-1} i.e. ν_1 CH_3 stretching region (b) 1280-1227 cm^{-1} i.e. ν_2 CH_3 bending region (c) 905-870 cm^{-1} i.e. ν_6 CH_3 rocking region. Bands denoted in green, pink and orange are assigned to CH_3I monomer, CH_3I dimer and CH_3I trimer, respectively.

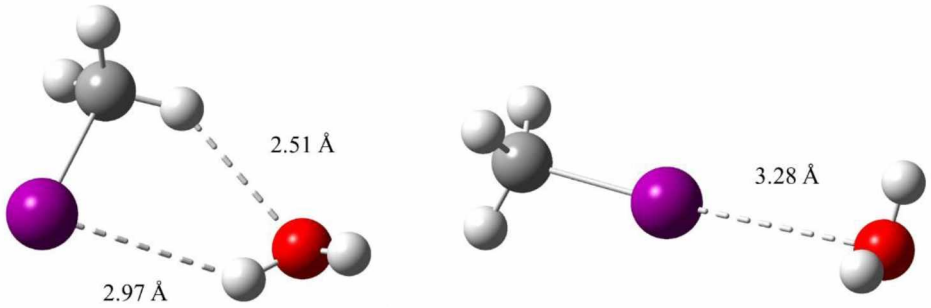

1:1a
$\Delta_r G°_{10K}$ = -13.5 kJ mol^{-1}

1:1b
$\Delta_r G°_{10K}$ = -7.5 kJ mol^{-1}

Fig. S4: ωB97X-D/ aug-cc-pVTZ-PP-predicted geometry (distances in Å) and Gibbs free energy (ΔG in kJ mol^{-1}) of $CH_3I.H_2O$ isomers.

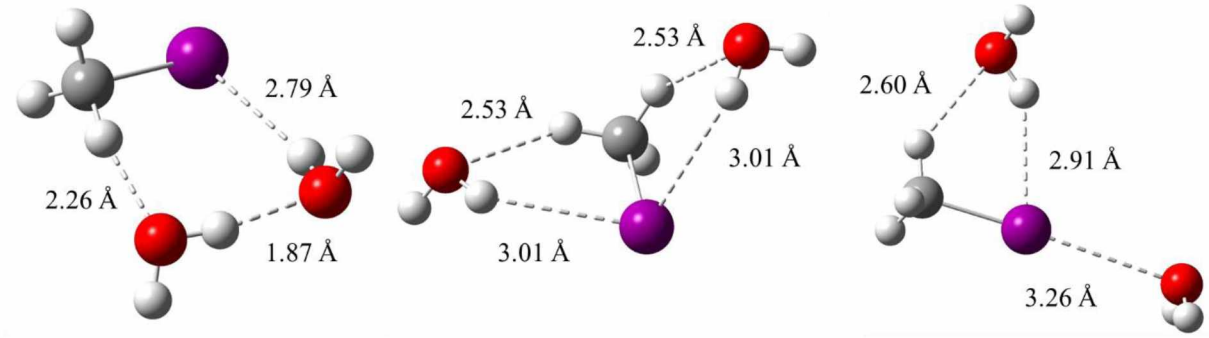

1:2a
$\Delta_r G°_{10K}$ = -45.0 kJ mol^{-1}

1:2b
$\Delta_r G°_{10K}$ = -25.3 kJ mol^{-1}

1:2c
$\Delta_r G°_{10K}$ = -21.61 kJ mol^{-1}

Fig. S5: ωB97X-D/ aug-cc-pVTZ-PP-predicted geometry (distances in Å) and Gibbs free energy (ΔG in kJ mol^{-1}) of $CH_3I.(H_2O)_2$ isomers.

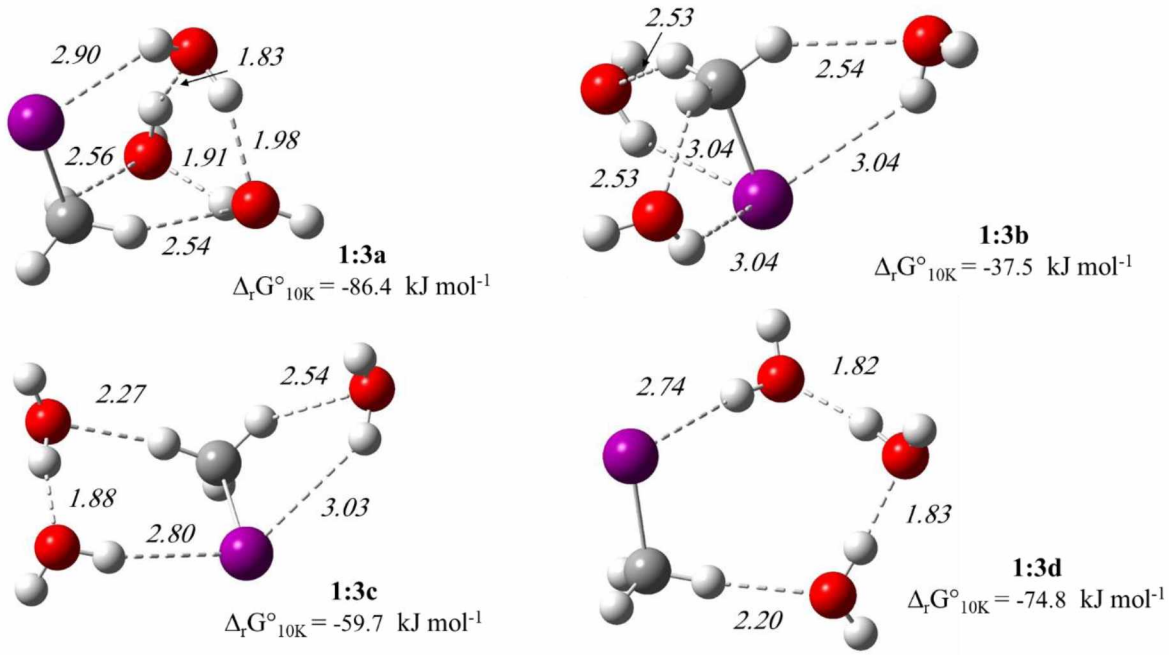

1:3a
$\Delta_r G°_{10K}$ = -86.4 kJ mol^{-1}

1:3b
$\Delta_r G°_{10K}$ = -37.5 kJ mol^{-1}

1:3c
$\Delta_r G°_{10K}$ = -59.7 kJ mol^{-1}

1:3d
$\Delta_r G°_{10K}$ = -74.8 kJ mol^{-1}

Fig. S6: ωB97X-D/ aug-cc-pVTZ-PP-predicted geometry (distances in Å) and Gibbs free energy (ΔG in kJ mol^{-1}) of $CH_3I.(H_2O)_3$ isomers.

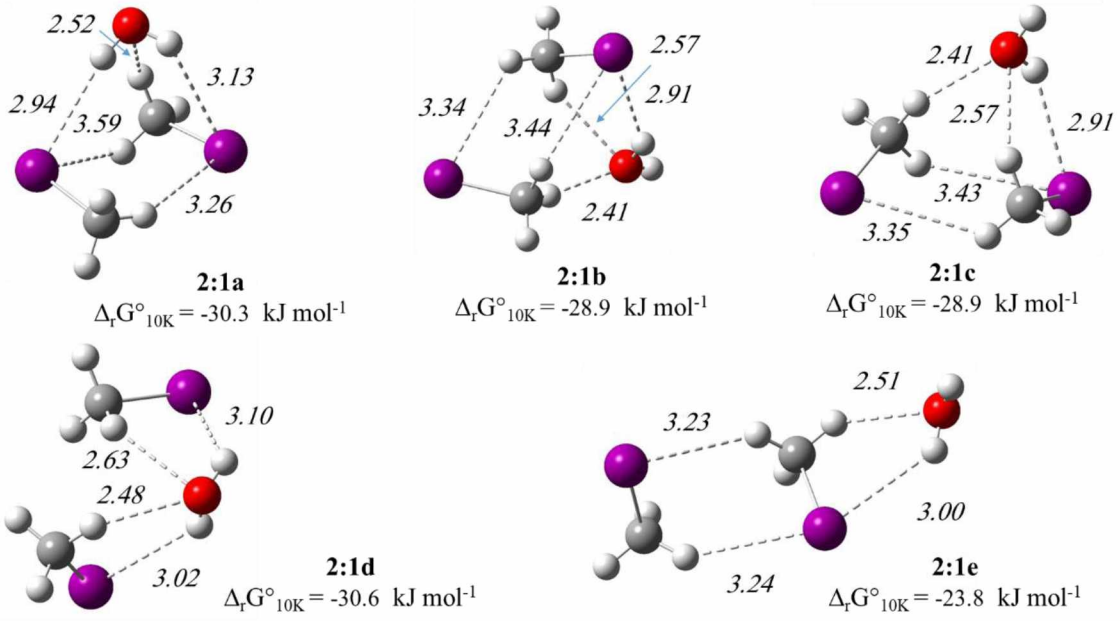

Fig. S7: ωB97X-D/ aug-cc-pVTZ-PP-predicted geometry (distances in Å) and Gibbs free energy (ΔG in kJ mol^{-1}) of $(CH_3I)_2.(H_2O)$ isomers.

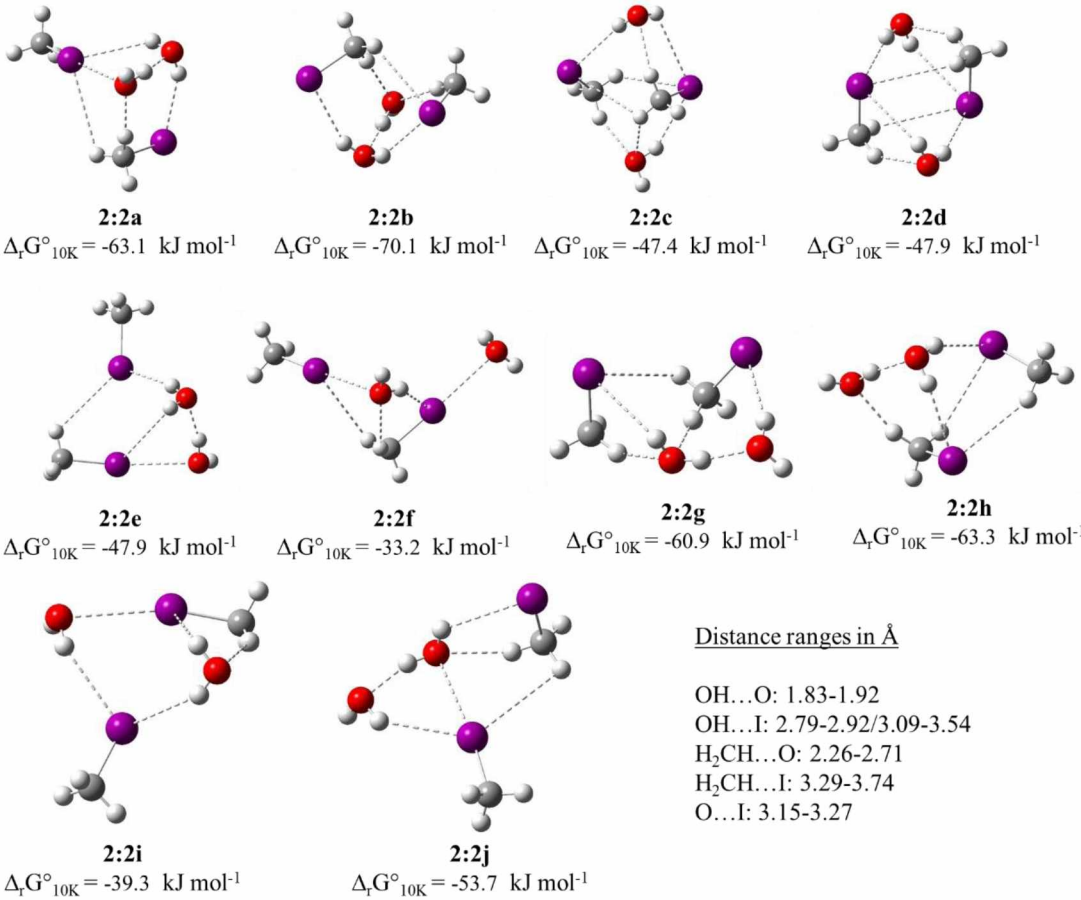

Fig. S8: ωB97X-D/ aug-cc-pVTZ-PP-predicted geometry (distances in Å) and Gibbs free energy (ΔG in kJ mol^{-1}) of $(CH_3I)_2.(H_2O)_2$ isomers.

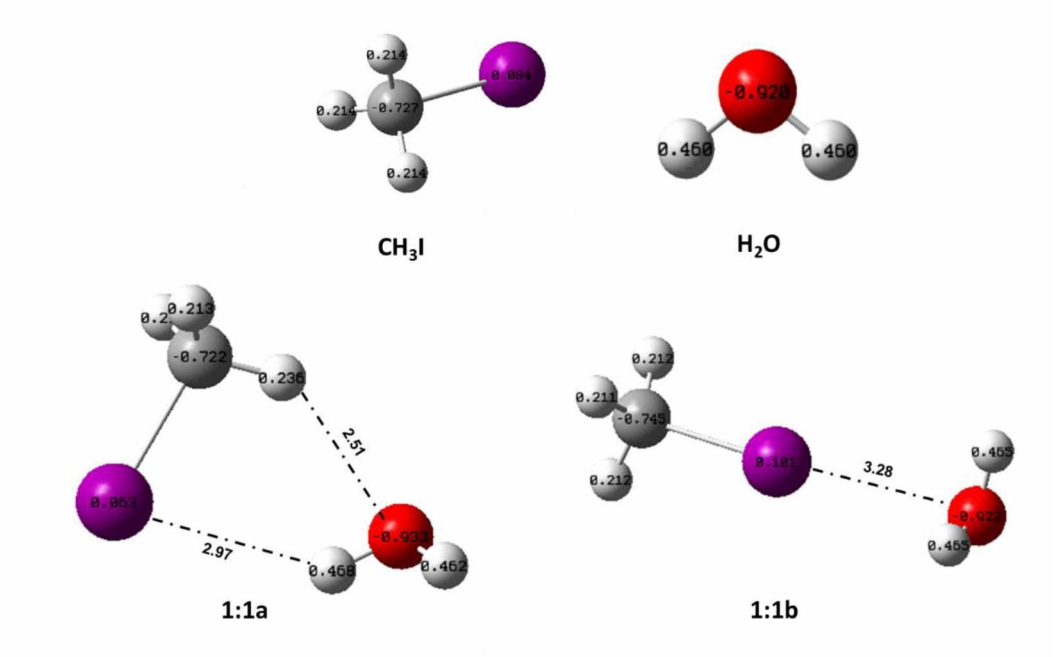

Fig. S9: Distribution of NBO charges calculated at ωB97X-D/aug-cc-pVTZ level of theory for CH_3I, H_2O monomers and 1:1a and 1:1b complexes.

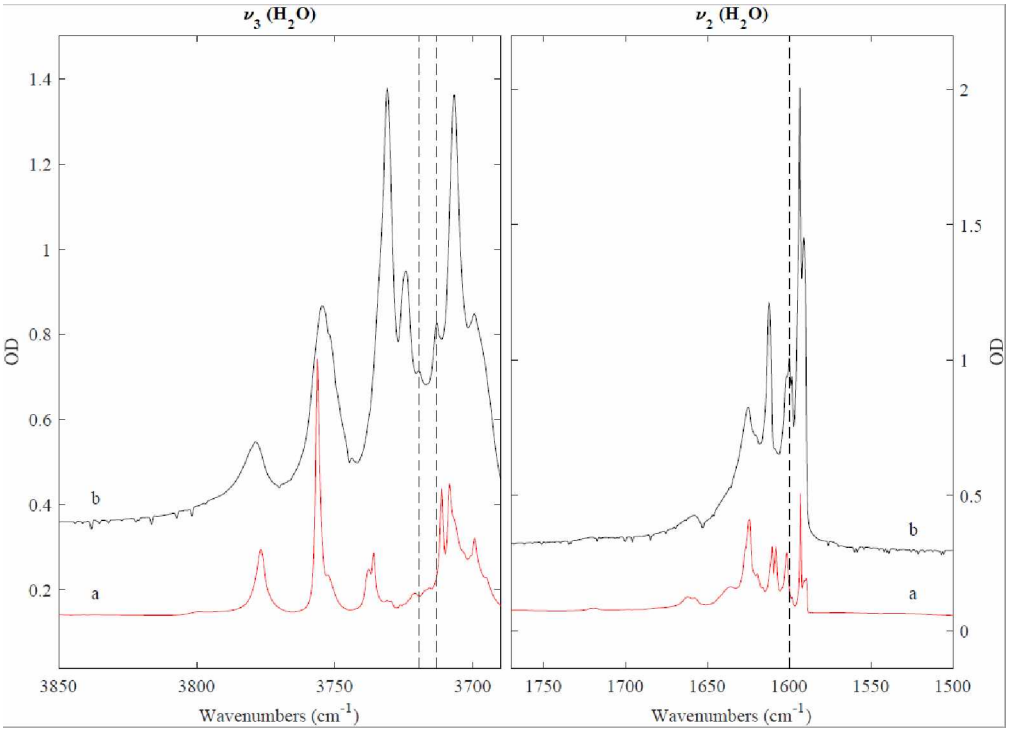

Fig. S10: IR spectra in the ν_3 (symmetric stretching) and ν_2 (bending mode) regions of pure water cluster matrix (trace (a)) (H_2O/Ar = 7/1000), recorded at 4 K, and of mixed CH_3I/H_2O/Ar = 1/25/1500, recorded at 10 K (trace (b) new bands are marked with dashed lines).

Table S1. Optimized Cartesian Coordinates of $(H_2O)_n$ at the ωB97X-D/aug–cc–pVTZ level of theory

(H_2O)

O	–0.000000	0.000000	0.116383
H	0.000000	0.760161	–0.465533
H	–0.000000	–0.760161	–0.465533

$(H_2O)_2$

O	1.501446	–0.000598	–0.120598
H	1.916104	0.003574	0.741310
H	0.551378	–0.000064	0.053544
O	–1.385260	0.000411	0.114636
H	–1.699478	–0.763555	–0.370726
H	–1.697491	0.761544	–0.376434

Table S2. Optimized Cartesian Coordinates of $(CH_3I)_n$ at the ωB97X-D/aug–cc–pVTZ level of theory

(CH_3I)

C	0.000000	0.000000	–1.811644
I	0.000000	0.000000	0.326414
H	0.000000	1.031350	–2.143367
H	0.893175	–0.515675	–2.143367
H	–0.893175	–0.515675	–2.143367

$(CH_3I)_2$ HH

C	–3.907754	0.390987	–0.004362
I	–1.838951	–0.154458	0.001166
H	–3.969591	1.472138	–0.040989
H	–4.366730	–0.053585	–0.879470
H	–4.355098	0.007545	0.905010
C	1.665941	1.816332	0.000879
I	2.243080	–0.243018	–0.000569
H	2.569710	2.413619	–0.019023
H	1.058971	1.986833	–0.880054
H	1.094765	1.995721	0.903781

$(CH_3I)_2$ HT

C	1.622437	1.814822	0.000071
I	2.278767	–0.220718	–0.000015
H	0.538611	1.804962	–0.001982
H	2.011550	2.285114	0.895105
H	2.014959	2.286406	–0.892798
C	–1.482055	–1.763383	0.000070
I	–2.304184	0.211418	–0.000015
H	–2.309355	–2.463006	–0.000137
H	–0.875177	–1.864681	–0.891350
H	–0.875788	–1.864529	0.891907

$(CH_3I)_3$ THT_1

C	–2.611265	–0.156029	1.535612
H	–3.674467	–0.082235	1.730068
I	–2.354844	–1.202688	–0.311660
H	–2.160561	0.822633	1.418122
H	–2.111858	–0.726937	2.309631
C	1.103445	–1.240263	1.647369
H	1.753062	–1.322161	2.510703
I	2.308466	–1.482244	–0.100793
H	0.355746	–2.024739	1.636964
H	0.645072	–0.259067	1.589717

C	0.423170	1.700963	−1.762384
H	0.003244	2.380145	−2.494538
I	0.241593	2.630053	0.156476
H	−0.126321	0.767960	−1.720854
H	1.477570	1.524966	−1.936626

$(CH_3I)_3$–THT_2

C	2.145148	2.734239	0.397215
H	2.178470	3.194791	1.377319
I	0.092032	2.376726	−0.085539
H	2.552316	3.394720	−0.358936
H	2.649296	1.774587	0.395383
C	0.925720	−1.532791	−1.411356
H	0.273384	−2.375321	−1.214532
I	2.454356	−1.524893	0.085833
H	1.410959	−1.630193	−2.374967
H	0.386654	−0.595555	−1.332725
C	−1.378208	−1.217054	1.430838
H	−1.875731	−1.182816	2.392580
I	−2.851214	−0.849020	−0.075398
H	−0.625893	−0.440256	1.348768
H	−0.949663	−2.195364	1.247436

Table S3. Optimized Cartesian Coordinates of $CH_3I.H_2O$ at the ωB97X-D/aug–cc–pVTZ level of theory

CH_3I_ (1:1a)

C	−0.324666	1.691645	−0.008427
I	0.637281	−0.222031	−0.001147
H	−1.392797	1.509590	−0.046959
H	−0.039582	2.202525	0.903298
H	0.022906	2.227418	−0.883518
O	−3.082563	−0.345960	0.081432
H	−2.262422	−0.835751	0.185006
H	−3.495515	−0.718337	−0.697934

CH_3I (1:1b)

C	2.307237	−0.003551	−0.166295
I	0.178576	0.001026	0.049239
H	2.667308	0.999157	0.032560
H	2.715483	−0.707898	0.549203
H	2.543533	−0.303803	−1.180597
O	−3.102335	−0.000221	0.013228
H	−3.205324	0.751192	−0.572008
H	−3.210251	−0.769953	−0.546874

Table S4. Optimized Cartesian Coordinates of $CH_3I.(H_2O)_2$ at the ωB97X-D/aug–cc–pVTZ level of theory

CH_3I (1:2a)

C	0.116256	1.741200	0.280616
H	−0.948043	1.638711	0.092753
H	0.319186	2.018187	1.308074
I	1.018017	−0.176580	−0.046812
H	0.583949	2.431321	−0.411423
O	−3.126561	1.052353	−0.116378
H	−3.710066	1.199234	−0.859808
H	−2.996516	0.092444	−0.074015
O	−2.372825	−1.667010	0.089172
H	−2.480960	−2.032587	0.967911

H	−1.424912	−1.518494	−0.008498

CH_3I (1:2b)

C	0.000343	0.997859	1.240818
H	−0.900298	1.556198	1.011883
H	0.000288	0.636026	2.261971
I	−0.000078	−0.724250	−0.039093
H	0.901257	1.555763	1.011877
O	−2.946397	1.544332	−0.472769
H	−3.768260	1.150397	−0.179493
H	−2.452615	0.821528	−0.867688
O	2.946091	1.543875	−0.472455
H	3.770948	1.152828	−0.183775
H	2.453218	0.819674	−0.865956

CH_3I (1:2c)

C	−1.682986	−1.368027	−0.060041
I	0.195580	−0.341787	0.019537
O	−2.695047	1.976821	−0.081435
H	−2.462800	−0.615086	−0.028316
H	−1.716504	−1.930080	−0.985919
H	−1.737091	−2.029032	0.797035
H	−1.751392	1.811066	−0.161677
H	−2.788982	2.456539	0.741744
O	3.092707	1.148174	0.009620
H	3.335933	1.102866	−0.915775
H	3.671701	0.526608	0.452207

Table S5. Optimized Cartesian Coordinates of $CH_3I.(H_2O)_3$ at the ωB97X-D/aug–cc–pVTZ Level of Theory

CH_3I (1:3a)

C	0.010512	−1.464690	0.213293
H	−0.612854	−1.208631	1.061957
H	−0.575667	−1.497340	−0.697415
I	1.470805	0.086950	−0.012056
H	0.548915	−2.390457	0.376729
O	−2.917972	−0.155402	1.427486
H	−3.582123	0.109208	2.062601
H	−2.532802	0.666126	1.068307
O	−1.856114	1.740086	−0.254743
H	−2.115655	1.094109	−0.928451
H	−0.894684	1.741489	−0.263691
O	−2.901353	−0.680713	−1.314662
H	−3.707041	−0.823556	−1.809960
H	−3.140314	−0.742902	−0.375521

CH_3I (1:3b)

C	−0.005267	0.001934	1.442340
H	1.032388	−0.030912	1.754539
H	−0.498362	0.919908	1.741535
I	0.009429	−0.003160	−0.706516
H	−0.556495	−0.881057	1.745340
O	3.408414	−0.202132	0.883067
H	2.949832	−0.137947	0.042091
H	3.769426	−1.088828	0.901001
O	−1.911022	−2.829204	0.862906
H	−2.854128	−2.664211	0.878937
H	−1.611164	−2.471901	0.023828

O	−1.544158	3.042614	0.855416
H	−1.361723	2.616753	0.014597
H	−0.963766	3.803873	0.878346

CH_3I (1:3c)

C	−0.288616	1.063986	1.180678
H	−1.090712	1.708947	0.839708
H	−0.382344	0.825398	2.233199
I	−0.511068	−0.782496	0.105452
H	0.693083	1.459272	0.939261
O	−2.962766	1.894174	−0.861011
H	−2.729856	0.972004	−0.991932
H	−2.702561	2.331617	−1.672028
O	2.831352	1.929167	0.325530
H	3.153499	2.649977	−0.214208
H	3.023054	1.122057	−0.175804
O	3.035139	−0.567788	−0.995759
H	2.105906	−0.801911	−0.889804
H	3.518433	−1.223400	−0.491497

CH_3I (1:3d)

C	0.724463	−1.626333	0.798241
H	1.390783	−2.407409	0.451906
H	0.833210	−1.461186	1.863477
I	1.330811	0.180462	−0.184809
H	−0.307395	−1.817155	0.517780
O	−3.599594	0.454128	−0.513019
H	−3.582593	0.704562	−1.436333
H	−3.011245	1.080383	−0.058692
O	−2.413831	−2.040049	−0.067579
H	−3.057099	−2.583321	0.385726
H	−2.865405	−1.194571	−0.234134
O	−1.716973	2.000965	0.836722
H	−1.576828	2.947628	0.829704
H	−0.859993	1.604241	0.637010

Table S6. Optimized Cartesian Coordinates of $(CH_3I)_2.H_2O$ at the ωB97X-D/aug–cc–pVTZ level of theory

2 CH_3I (2:1a)

C	−1.575315	0.977955	1.456682
I	−2.262936	−0.364071	−0.064336
8	−0.197901	2.590166	−1.248997
H	−1.190055	1.855777	0.949939
H	−2.423576	1.213604	2.088018
H	−0.796625	0.466645	2.009733
H	−0.836154	1.964730	−1.598248
H	0.558742	2.048659	−1.007545
C	1.668714	−1.620225	−1.017960
H	2.119107	−2.521154	−0.619153
I	2.281513	0.009132	0.225408
H	2.020281	−1.417040	−2.022285
H	0.586517	−1.667193	−0.977615

2 CH_3I (2:1b)

C	1.114383	−0.416188	1.418991
I	2.532677	−0.393328	−0.186788
O	0.990773	2.894500	0.406319
H	0.724805	0.591081	1.514019

H	0.332060	−1.117573	1.154882
H	1.641221	−0.727223	2.312972
H	1.693452	2.389679	−0.012888
H	1.420559	3.654417	0.798844
C	−1.336739	0.913093	−1.110691
H	−1.902725	1.370256	−1.913501
I	−2.702943	−0.251959	0.054882
H	−0.581666	0.239949	−1.500442
H	−0.895615	1.662207	−0.463247

2 CH_3I (2:1c)

C	1.101742	−0.433871	1.395182
I	2.551156	−0.386601	−0.181899
O	0.974577	2.887192	0.404833
H	0.697171	0.567854	1.486407
H	0.333887	−1.144454	1.113696
H	1.614564	−0.741685	2.298382
H	1.685426	2.387834	−0.007053
H	1.398516	3.633078	0.829335
C	−1.329928	0.885948	−1.115426
H	−0.896740	1.648015	−0.477799
I	−2.717338	−0.249051	0.054642
H	−1.881829	1.326529	−1.937093
H	−0.570805	0.202390	−1.478472

2 CH_3I (2:1d)

C	2.411190	1.212758	1.149612
I	2.311909	−0.457949	−0.185928
O	0.011015	2.384778	−0.973575
H	1.712084	1.956599	0.783797
H	2.137140	0.859098	2.136602
H	3.429219	1.582844	1.136632
H	0.424145	1.603317	−1.350322
H	−0.928898	2.233724	−1.095605
C	−1.236576	0.254033	1.538528
H	−1.866087	0.481385	2.390492
I	−2.515476	−0.242118	−0.102814
H	−0.649901	1.112877	1.232491
H	−0.604421	−0.605273	1.728977

2 CH_3I (2:1e)

C	1.982056	−1.143374	1.168453
I	2.618939	0.365834	−0.206205
H	1.835033	−0.671597	2.132800
H	1.055835	−1.561256	0.790385
H	2.760794	−1.894890	1.218089
C	−1.297628	0.888439	1.084621
I	−1.912271	−0.710726	−0.201186
H	−2.076099	1.642061	1.044678
H	−1.190142	0.479736	2.082326
H	−0.352840	1.260972	0.704926
O	−4.363495	2.092095	0.120870
H	−4.450018	2.622727	−0.671386
H	−4.234609	1.194386	−0.195520

Table S7. Optimized Cartesian Coordinates of $(CH_3I)_2.(H_2O)_2$ at the ωB97X-D/aug–cc–pVTZ level of theory

2 CH_3I (2:2a)

C	3.081757	−1.899383	0.573459
I	2.186556	−0.088214	−0.131107

H	3.781850	–1.646030	1.360920
H	2.292403	–2.540078	0.948874
H	3.592992	–2.365730	–0.260634
C	–1.543864	0.047054	–1.716193
I	–2.501840	–0.446960	0.136091
H	–2.325735	0.160615	–2.457626
H	–0.990122	0.967665	–1.566115
H	–0.880539	–0.773985	–1.959882
O	–0.268159	2.020701	1.813847
H	0.439033	1.383295	1.946965
H	–1.041157	1.477300	1.623846
O	0.468182	2.577566	–0.830998
H	0.201208	2.577418	0.103395
H	0.812560	3.451574	–1.010321

2 CH_3I (2:2b)

C	–2.524571	0.921063	–1.292330
I	–2.283772	–0.642602	0.153657
H	–3.538010	1.292139	–1.197452
H	–1.792814	1.691085	–1.070181
H	–2.360696	0.480533	–2.268750
C	1.299805	0.246935	–1.603239
I	2.500446	–0.433548	0.034409
H	1.937258	0.269928	–2.479123
H	0.491495	–0.465656	–1.720633
H	0.929720	1.234744	–1.348314
O	0.105059	1.581876	2.025227
H	0.875145	1.037911	1.825614
H	–0.640282	0.981596	1.921561
O	–0.112062	3.029100	–0.344552
H	–0.020382	2.649547	0.546927
H	0.039502	3.968343	–0.249154

2 CH_3I (2:2c)

C	–1.395242	–0.386223	1.631930
I	–2.316589	–0.088136	–0.281590
H	–2.185821	–0.375265	2.372565
H	–0.894045	–1.346413	1.583388
H	–0.697731	0.430656	1.777365
C	1.514736	1.323279	–1.252202
I	2.428441	–0.087425	0.073748
H	2.291389	1.700864	–1.906434
H	0.749727	0.796074	–1.809971
H	1.083432	2.107222	–0.640349
O	0.038000	–3.077137	0.113373
H	0.725288	–2.426543	–0.059202
H	–0.613213	–2.927790	–0.573795
O	–0.628466	3.005650	0.715742
H	–1.051796	3.779950	1.086562
H	–1.328587	2.515563	0.274196

2 CH_3I (2:2d)

C	1.661247	0.828440	1.608611
I	2.227108	–0.154645	–0.208699
H	2.536557	0.859352	2.246013
H	1.318568	1.819313	1.332110
H	0.863950	0.246068	2.055005
C	–1.659685	–0.854195	–1.605328
I	–2.227386	0.154637	0.197262
H	–2.535122	–0.896560	–2.241900

H	–0.863609	–0.276917	–2.060336
H	–1.315054	–1.840294	–1.314448
O	0.181839	3.101143	–0.412147
H	–0.568556	2.507934	–0.313831
H	0.730712	2.687795	–1.080565
O	–0.182278	–3.080201	0.475843
H	–0.733752	–2.616985	1.108713
H	0.575213	–2.502256	0.346095

2 CH_3I (2:2e)

C	–4.058086	–0.129304	0.097990
I	–1.933695	–0.228816	–0.151890
H	–4.421201	0.714972	–0.475828
H	–4.476995	–1.058302	–0.270287
H	–4.264833	–0.000939	1.153758
C	1.830716	–2.375832	0.587534
I	1.998716	–0.342122	–0.060119
H	2.514283	–2.525747	1.415235
H	0.805807	–2.546122	0.897922
H	2.090624	–3.017233	–0.246623
O	1.929789	2.719045	–0.800768
H	1.600115	2.990630	–1.656703
H	1.205952	2.879918	–0.176670
O	–0.047681	2.723993	1.259234
H	–0.692854	2.081861	0.944410
H	0.500328	2.227199	1.870403

2 CH_3I (2:2f)

C	–3.833642	1.047303	–1.195959
I	–2.449162	0.128178	0.152330
H	–3.273725	1.674606	–1.879900
H	–4.354911	0.262890	–1.732354
H	–4.528561	1.640434	–0.612826
C	0.947089	–1.788523	–1.027733
I	2.221732	–0.232840	–0.291313
H	1.568427	–2.513269	–1.540633
H	0.444540	–2.230925	–0.175195
H	0.229044	–1.335010	–1.700423
O	4.113312	2.245794	0.685052
H	3.730172	2.934681	0.140729
H	4.952419	2.037625	0.272674
O	–0.288164	–1.127528	2.188496
H	0.485734	–0.640239	1.887285
H	–0.481208	–0.782533	3.060503

2 CH_3I (2:2g))

C	–2.601810	0.742400	1.487567
I	–2.513396	–0.342873	–0.356218
H	–2.406729	0.040126	2.289572
H	–1.843957	1.516442	1.438407
H	–3.596782	1.162551	1.572402
C	1.003333	–0.251107	1.525499
I	2.331883	–0.772027	–0.070663
H	1.593971	–0.177210	2.430850
H	0.544087	0.695111	1.256433
H	0.268364	–1.044644	1.594193
O	–0.189304	2.598415	0.126178
H	0.713328	2.816875	–0.151207
H	–0.606207	2.232354	–0.655671
O	2.518261	2.859726	–0.682463

H	2.748410	1.924341	–0.639240
H	3.164909	3.310825	–0.139160

2 CH_3I (2:2h)

C	1.941760	–1.802726	0.798900
I	2.373788	0.021359	–0.232776
H	2.477977	–2.597155	0.293986
H	2.279594	–1.690087	1.821998
H	0.869725	–1.955338	0.749506
C	–1.641265	0.417592	–1.619113
I	–2.133358	–0.782851	0.088551
H	–2.353801	0.167172	–2.395911
H	–1.716053	1.456945	–1.315400
H	–0.629827	0.158066	–1.908520
O	–0.216884	1.932432	1.783529
H	0.624748	1.634716	1.424105
H	–0.795386	1.168178	1.689988
O	–1.344665	3.452697	–0.316925
H	–0.947970	3.054199	0.473961
H	–1.862379	4.192168	–0.001332

2 CH_3I (2:2i)

C	–4.033673	–0.180420	0.015353
I	–1.910671	–0.043831	–0.226804
H	–4.474475	0.707770	–0.421343
H	–4.367442	–1.073627	–0.499145
H	–4.244132	–0.239590	1.076456
C	2.688375	–1.587228	–0.861775
I	2.056453	0.296860	–0.063986
H	2.513839	–1.569589	–1.931096
H	3.743272	–1.703090	–0.642370
H	2.095135	–2.353213	–0.374089
O	0.255945	2.965542	0.954840
H	–0.503782	2.378535	0.928786
H	0.234393	3.428417	0.116486
O	0.366945	–2.722840	1.464830
H	–0.419859	–2.376039	1.037779
H	0.785246	–1.945801	1.841573

2 CH_3I (2:2j)

C	3.296608	–2.031918	–0.402920
I	1.934437	–0.449623	0.068795
H	4.132718	–1.976172	0.284289
H	2.766874	–2.970606	–0.289493
H	3.626854	–1.898921	–1.426475
C	–1.808918	–0.399049	1.619179
I	–2.717930	–0.127822	–0.300441
H	–1.100880	0.410749	1.753334
H	–2.598529	–0.372333	2.360523
H	–1.309238	–1.360217	1.607438
O	0.086782	2.148846	0.585116
H	–0.588640	2.106092	–0.094790
H	0.806468	2.676086	0.209649
O	2.529644	3.188402	–0.469390
H	2.848524	2.283797	–0.549461
H	3.083421	3.593947	0.198826

620

Table S8. Calculated wavenumbers (cm^{-1}) and intensities (I in km/mol) of CH_3I monomer, HH and HT dimers and THT and TTH trimers. The IR bands are predicted at the ωB97X-D/aug-cc-pVTZ-PP level of theory. The frequency shifts are calculated with respect to the monomer position ($\Delta\nu = \nu - \nu_{monomer}$).

Vibrational Modes		CH_3I	$(CH_3I)_2$ dimers				$(CH_3I)_3$ trimers			
		monomer	HT	Δν	HH	Δν	THT	Δν	TTH	Δν
v4	C-H stretching degenerated	3214 (0)	3221 (0)	7	3214 (0)	0	3221 (0)	7	3215 (1)	1
			3217 (1)	3	3214 (1)	0	3216 (1)	2	3214 (0)	0
			3215 (0)	1	3211 (1)	-3	3214 (1)	0	3213 (2)	-1
			3214 (1)	0	3211 (1)	-3	3213 (1)	-1	3211 (0)	-3
							3210 (1)	-4	3210 (2)	-4
							3206 (1)	-8	3206 (1)	-8
v1	Sym CH_3 stretching	3101 (11)	3103 (8)	2	3100 (9)	-1	3101 (8)	0	3097 (10)	-4
			3099 (13)	-2	3100 (14)	-1	3097 (10)	-4	3096 (10)	-5
							3094 (14)	-7	3093 (11)	-8
v5	CH_3 deformation degenerated	1477 (6)	1485 (14)	8	1477 (8)	0	1482 (3)	6	1486 (7)	9
			1480 (7)	3	1477 (6)	0	1479 (12)	2	1485 (3)	8
			1477 (5)	0	1474 (10)	-3	1477 (8)	0	1478 (7)	1
			1474 (2)	-3	1473 (12)	-4	1474 (2)	-3	1477 (7)	0
							1473 (12)	-4	1474 (3)	-3
							1470 (2)	-7	1470 (9)	-7
v2	Sym CH_3 deformation	1297 (23)	1300 (41)	3	1297 (12)	0	1300 (39)	3	1305 (2)	8
			1297 (1)	0	1296 (40)	-1	1297 (10)	0	1296 (46)	-1
							1295 (16)	-2	1294 (27)	-3
v6	CH_3 rocking degenerated	903 (5)	913 (15)	10	906 (7)	3	921 (8)	18	914 (7)	11
			910 (4)	7	905 (7)	2	917 (15)	14	911 (10)	7
			909 (4)	6	902 (3)	-1	911 (7)	8	909 (15)	6
			908 (5)	5	901 (4)	-2	910 (7)	7	907 (3)	4
							906 (10)	3	906 (7)	3
							904 (2)	1	905 (4)	2

Table S9. Calculated wavenumbers (cm^{-1}) and intensities (I in km/mol) of $CH_3I.H_2O$ complexes compared to the calculated wavenumber (cm^{-1}) and intensities (I) of CH_3I monomer and H_2O monomer and dimer. The IR bands are predicted at the ωB97X-D/aug-cc-pVTZ-PP level of theory. The frequency shifts are calculated with respect to the monomer position ($\Delta\nu = \nu - \nu_{monomer}$).

Vibrational Mode		**H_2O monomer**	**H_2O dimer**	**CH_3I monomer**	**CH_3I-H_2O (1 :1a)**	**Δν**	**CH_3I-H_2O (1 :1b)**	**Δν**
ν_3 H_2O	anti sym stretching	3986 (63)	3974 (85)		3958 (106)	-28	3975 (63)	-11
			3954 (86)					
ν_1 H_2O	sym stretching	3879(5)	3871 (11)		3838 (48)	-41	3869 (11)	-10
			3751 (339)					
ν_2 H_2O	bending	1637 (63)	1658 (39)		1642 (49)	5	1636 (67)	-1
			1637 (94)					
ν_4	C-H stretching			3214 (0)	3215 (0)	1	3207 (1)	-7
					3213 (5)	-1	3207 (1)	-7
ν_1	Sym CH_3 stretching			3101 (11)	3096 (12)	-5	3097 (15)	-4
ν_5	CH_3 deformation			1477 (6)	1484 (5)	7	1478 (6)	1
					1474 (4)	-3	1478 (6)	1
ν_2	Sym CH_3 deformation			1297 (23)	1301 (22)	4	1296 (23)	-1
ν_6	CH_3 rocking			903 (5)	925 (7)	22	900 (5)	-3
					909 (5)	6	899 (5)	-4

Table S10. Calculated wavenumbers (cm^{-1}) and intensities (I) of $CH_3I.(H_2O)_2$ complexes compared to the calculated wavenumber (cm^{-1}) and intensities (I in km/mol) of CH_3I monomer and H_2O monomer and dimer. The IR bands are predicted at the ωB97X-D/aug-cc-pVTZ-PP level of theory. The frequency shifts are calculated with respect to the monomer position ($\Delta\nu = \nu - \nu_{monomer}$)

Vibrational Mode		**H_20 monomer**	**H_2O dimer**	**CH_3I monomer**	**CH_3I-$2H_2O$ 1 :2a**	**Δν**	**νCH_3I-$2H_2O$ 1 :2b**	**Δν**	**CH_3I-$2H_2O$ 1 :2c**	**Δν**
ν_3 H_2O	anti sym stretching	3986 (63)	3974 (85)		3950 (74)	-36	3960 (18)	-26	3978 (66)	-8
			3954 (86)		3940 (131)	-46	3960 (188)	-26	3955 (107)	-31
ν_1 H_2O	sym stretching	3879(5)	3871 (11)		3782 (256)	-97	3845 (35)	-34	3872 (13)	-7
			3751 (339)		3674 (358)	-205	3845 (35)	-34	3828 (77)	-51
ν_2 H_2O	bending	1637 (63)	1658 (39)		1662 (40)	25	1639 (92)	2	1642 (45)	5
			1637 (94)		1638 (61)	1	1638 (9)	1	1636 (73)	-1
ν_4	C-H stretching			3214 (0)	3215 (1)	1	3216 (1)	2	3210 (1)	-4
					3205 (34)	-9	3215 (14)	1	3209 (2)	-5
ν_1	C-H stretching			3101 (11)	3087 (28)	-14	3093 (9)	-8	3095 (14)	-6
ν_5				1477 (6)	1491 (4)	14	1484 (3)	7	1484 (4)	7
	Sym CH_3 stretching				1475 (4)	-2	1478 (2)	4	1476 (4)	-1
ν_2	CH_3 deformation			1297 (23)	1312 (27)	5	1303 (20)	6	1300 (21)	3
ν_6				903 (5)	935 (4)	31	937 (9)	33	921 (6)	18
					917 (5)	14	925 (5)	22	905 (4)	2

Table S11. Calculated wavenumbers (cm^{-1}) and intensities (I in km/mol) of $CH_3I.(H_2O)_3$ complexes compared to the calculated wavenumber (cm^{-1}) and intensities (I) of CH_3I monomer and H_2O monomer and dimer. The IR bands are predicted at the ωB97X-D/aug-cc-pVTZ-PP level of theory. The frequency shifts are calculated with respect to the monomer position ($\Delta\nu = \nu - \nu_{monomer}$).

Vibrational modes	**H_2O monomer**	**H_2O Dimer**	**CH_3I monomer**	**CH_3I-3H_2O 1 :3a**	**Δν**	**CH_3I-3H_2O 1 :3b**	**Δν**	**CH_3I-3H_2O 1 :3c**	**Δν**	**CH_3I-3H_2O 1 :3d**	**Δν**
ν_3 H_2O	3986 (63)	3974 (85)		3950 (60)	-36	3962 (54)	-24	3961 (94)	-25	3949 (74)	-37
		3954 (86)		3948 (99)	-38	3961 (124)	-25	3951 (71)	-35	3948 (132)	-38
				3861 (205)	-125	3960 (119)	-26	3941 (140)	-45	3943 (78)	-43
ν_1 H_2O	3879(5)	3871 (11)		3716 (294)	-63	3849 (19)	-30	3848 (29)	-31	3761 (354)	-118
		3751 (339)		3663 (358)	-216	3848 (32)	-31	3788 (246)	-91	3660 (499)	-219
				3557 (276)	-322	3848 (32)	-31	3680 (342)	-199	3606 (545)	-273
ν_2 H_2O	1637 (63)	1658 (39)		1669 (27)	32	1640 (27)	3	1661 (40)	24	1677 (36)	40
		1637 (94)		1653 (138)	16	1640 (27)	3	1640 (74)	3	1662 (32)	25
				1647 (58)	10	1638 (94)	1	1639 (37)	2	1636 (76)	-1
ν_4 CH_3I			3214 (0)	3219 (2)	5	3216 (12)	2	3216 (2)	2	3215 (0)	1
				3218 (2)	4	3213 (13)	-1	3206 44)	-8	3199 (50)	-15
ν_1 CH_3I			3101 (11)	3101 (6)	0	3088 (2)	-13	3085 (18)	-16	3079 (47)	-25
ν_5 CH_3I			1477 (6)	1485 (21)	8	1484 (1)	7	1493 (3)	16	1491 (5)	14
				1475 (7)	-2	1484 (2)	7	1476 (3)	-1	1474 (4)	-3
ν_2 CH_3I			1297 (23)	1310 (27)	13	1305 (20)	8	1314 (26)	17	1316 (28)	19
ν_6 CH_3I			903 (5)	918 (5)	15	946 (7)	44	951 (5)	48	940 (3)	37
				916 (11)	13	945 (7)	43	929 (5)	26	919 (5)	16

Table S12. Calculated wavenumbers (cm^{-1}) and intensities (I in km/mol) of $(CH_3I)_2.(H_2O)$ complexes compared to the calculated wavenumber (cm^{-1}) and intensities (I) of CH_3I monomer and H_2O monomer and dimer. The IR bands are predicted at the ωB97X-D/aug-cc-pVTZ-PP level of theory. The frequency shifts are calculated with respect to the monomer position ($\Delta\nu = \nu - \nu_{monomer}$).

Vibrational modes	**H_2O monomer**	**H_2O dimer**	**CH_3I monomer**	**$2CH_3I$-H_2O 2 :1a**	**Δν**	**$2CH_3I$-H_2O 2 :1b**	**Δν**	**$2CH_3I$-H_2O 2 :1c**	**Δν**	**$2CH_3I$-H_2O 2 :1d**	**Δν**	**$2CH_3I$-H_2O 2 :1d**	**Δν**
ν_3 H_2O	3986 (63)	3974 (85)		3925 (106)	-61	3957 (114)	-29	3957 (114)	-29	3925 (106)	-61	3959 (103)	-27
		3954 (86)											
ν_1 H_2O	3879(5)	3871 (11)		3825 (84)	-54	3825 (65)	-54	3825 (66)	-54	3833 (28)	-46	3842 (40)	-32
		3751 (339)											
ν_2 H_2O	1637 (63)	1658 (39)		1643 (70)	6	1634 (63)	-3	1633 (61)	-4	1646 (71)	9	1640 (49)	3
		1637 (94)											
ν_4 CH_3I			3214 (0)	3217 (1)	3	3218 (0)	4	3218 (0)	3	3214 (2)	0	3213 (3)	-1
				3216 (0)	2	3217 (8)	3	3216 (9)	2	3214 (0)	0	3213 (1)	-1
				3212 (4)	-2	3215 (2)	1	3214 (1)	0	3212 (2)	-2	3210 (1)	-4
				3211 (2)	-3	3209 (1)	-5	3209 (2)	-5	3211 (2)	-1	3208 (7)	-6
ν_1 CH_3I			3101 (11)	3097 (11)	-4	3099 (4)	-2	3098 (4)	-3	3097 (16)	-4	3098 (9)	-3
				3095 (11)	-6	3096 (7)	-5	3096 (7)	-5	3096 (3)	-5	3091 (7)	-10
ν_5 CH_3I			1477 (6)	1483 (11)	6	1496 (7)	19	1495 (6)	18	1488 (3)	11	1484 (5)	7
				1477 (3)	0	1483 (25)	6	1482 (28)	4	1481 (19)	4	1481 (3)	4
				1473 (2)	-4	1477 (8)	0	1478 (8)	1	1475 (10)	-2	1478 (9)	1
				1469 (8)	-8	1472 (12)	-5	1474 (9)	-2	1470 (7)	-7	1472 (9)	-5
ν_2 CH_3I			1297 (23)	1302 (35)	5	1308 (10)	11	1307 (8)	10	1302 (16)	5	1302 (27)	5
				1297 (5)	0	1301 (45)	0	1301 (48)	4	1298 (28)	1	1297 (21)	0
ν_6 CH_3I			903 (5)	926 (6)	23	924 (8)	21	925 (8)	22	925 (8)	22	930 (12)	27
				916 (11)	13	914 (2)	11	913 (5)	10	921 (6)	18	915 (4)	12
				913 (7)	10	913 (5)	10	913 (3)	10	910 (8)	7	911 (8)	7
				908 (4)	5	910 (7)	7	908 (7)	5	907 (5)	4	904 (6)	1

Table S13. Calculated wavenumbers (cm^{-1}) and intensities (I in km/mol) of $(CH_3I)_2.(H_2O)_2$ complexes compared to the calculated wavenumber (cm^{-1}) and intensities (I) of CH_3I monomer and H_2O monomer and dimer. The IR bands are predicted at the ωB97X-D/aug-cc-pVTZ-PP level of theory. The frequency shifts are calculated with respect to the monomer position ($\Delta\nu = \nu - \nu_{monomer}$).

Vibrational modes	**H_2O monomer**	**H_2O dimer**	**CH_3I monomer**	**$2CH_3I$-$2H_2O$ 2 :2a**	**Δν**	**$2CH_3I$-$2H_2O$ 2 :2b**	**Δν**	**$2CH_3I$-$2H_2O$ 2 :2c**	**Δν**	**$2CH_3I$-$2H_2O$ 2 :2d**	**Δν**	**$2CH_3I$-$2H_2O$ 2 :2e**	**Δν**
ν_3 H_2O	3986 (63)	3974 (85)		3949 (77)	-37	3950 (74)	-36	3954 (126)	-28	3937 (146)	-49	3948 (74)	-38
		3954 (86)		3888 (164)	-98	3864 (235)	-122	3937 (94)	-39	3934 (29)	-52	3922 (111)	-64
ν_1 H_2O	3879(5)	3871 (11)		3793 (152)	-86	3787 (142)	-92	3818 (151)	-61	3823 (159)	-56	3803 (156)	-76
		3751 (339)		3631 (310)	-248	3607 (370)	-266	3814 (58)	-65	3822 (18	-57	3685 (318)	-194
ν_2 H_2O	1637 (63)	1658 (39)		1655 (49)	18	1665 (42)	28	1643 (42)	6	1642 (3)	5	1665 (39)	32
		1637 (94)		1645 (81)	8	1646 (82)	9	1631 (57)	-6	1642 (136)	5	1649 (82)	12
ν_4 CH_3I			3214 (0)	3217 (3)	3	3213 (3)	-1	3216 (1)	2	3219 (1)	5	3213 (0)	1
				3213 (17)	-1	3211 (4)	-3	3215 (10)	1	3218 (1)	4	3213 (0)	-1
				3208 (1)	-6	3209 (24)	-5	3214 (11)	0	3216 (8)	2	3206 (1)	-8
				3208 (1)	-6	3206 (13)	-8	3213 (1)	-1	3213 (7)	-1	3203 (1)	-11
ν_1 CH_3I			3101 (11)	3098 (13)	-3	3091 (26)	-10	3096 (10)	-5	3097 (11)	-4	3100 (12)	-1
				3095 (15)	-6	3088 (10)	-13	3092 (9)	-9	3095 (12)	-6	3095 (16)	-6
ν_5 CH_3I			1477 (6)	1492 (13)	15	1496 (4)	19	1486 (20)	9	1488 (16)	11	1478 (4)	1
				1478 (5)	1	1486 (13)	9	1482 (7)	5	1486 (4)	9	1478 (3)	1
				1477 (6)	0	1476 (7)	-1	1473 (14)	-4	1471 (9)	-6	1476 (7)	-1
				1475 (8)	-2	1473 (9)	-4	1472 (2)	-5	1470 (2)	-7	1476 (7)	-1
ν_2 CH_3I			1297 (23)	1312 (28)	15	1312 (17)	15	1304 (36)	7	1303 (37)	6	1296 (29)	-1
				1296 (21)	-1	1307 (34)	10	1304 (12)	7	1300 (0)	3	1296 (22)	-1
ν_6 CH_3I			903 (5)	931 (5)	28	932 (5)	29	937 (7)	34	932 (2)	29	902 (4)	-1
				917 (6)	14	932 (5)	29	922 (4)	19	931 (10)	28	901 (5)	-2
				901 (3)	-2	916 (9)	13	921 (7)	18	913 (9)	10	900 (6)	-3
				900 (6)	-3	914 (4)	11	914 (9)	11	913 (6)	10	898 (3)	-5

654 Table S13. (continued)

Vibrational modes	**H_2O monomer**	**H_2O dimer**	**CH_3I monomer**	**$2CH_3I$-$2H_2O$ 2 :2f**	**Δν**	**$2CH_3I$-$2H_2O$ 2 :2g**	**Δν**	**$2CH_3I$-$2H_2O$ 2 :2h**	**Δν**	**$2CH_3I$-$2H_2O$ 2 :2i**	**Δν**	**$2CH_3I$-$2H_2O$ 2 :2j**	**Δν**
ν_3 H_2O	3986 (63)	3974 (85)		3977 (64)	-19	3945 (132)	-41	3951 (77)	-35	3955 (102)	-31	3946 (129)	-40
		3954 (86)		3950 (122)	-36	3911 (106)	-75	3870 (200)	-116	3935 (83)	-51	3901 (173)	-85
ν_1 H_2O	3879(5)	3871 (11)		3871 (12)	-8	3782 (236)	-97	3794 (134)	-85	3844 (44)	5	3817 (112)	-62
		3751 (339)		3803 (132)	-76	3683 (360)	-196	3659 (411)	-200	3843 (46)	4	3710 (288)	-169
ν_2 H_2O	1637 (63)	1658 (39)		1638 (67)	1	1672 (59)	35	1663 (37)	26	1646 (100)	9	1653 (60)	16
		1637 (94)		1636 (65)	-1	1635 (36)	-2	1646 (120)	9	1639 (63)	2	1638 (45)	1
ν_4 CH_3I			3214 (0)	3217 (2)	3	3214 (5)	0	3218 (0)	4	3215 (0)	1	3221 (4)	7
				3210 (1)	-4	3212 (1)	-2	3216 (0)	2	3214 (0)	0	3216 (2)	2
				3206 (1)	-8	3210 (5)	-4	3209 (30)	-5	3210 (0)	-4	3209 (1)	-5
				3205 (1)	-9	3201 (16)	-13	3206 (3)	-8	3207 (3)	-7	3208 (1)	-7
ν_1 CH_3I			3101 (11)	3099 (10)	-2	3094 (17)	-7	3094 (11)	-7	3101 (10)	0	3100 (11)	-1
				3096 (16)	-5	3084 (15)	-9	3091 (24)	-10	3093 (15)	-8	3098 (13)	-3
ν_5 CH_3I			1477 (6)	1482 (16)	5	1490 (6)	13	1491 (7)	14	1487 (4)	10	1506 (8)	29
				1478 (6)	1	1483 (16)	6	1477 (4)	0	1476 (6)	-1	1478 (7)	1
				1478 (5)	1	1475 (6)	-2	1474 (3)	-3	1476 (7)	-1	1478 (11)	1
				1474 (7)	-3	1469 (10)	-8	1471 (4)	-6	1474 (4)	-3	1477 (0)	0
ν_2 CH_3I			1297 (23)	1302 (23)	5	1306 (26)	9	1310 (27)	13	1298 (14)	1	1304 (26)	7
				1295 (26)	-2	1301 (25)	4	1298 (13)	2	1296 (41)	-1	1296 (26)	-1
ν_6 CH_3I			903 (5)	921 (5)	18	937 (5)	34	934 (4)	31	920 (7)	17	935 (8)	32
				907 (7)	4	926 (9)	23	920 (10)	17	907 (5)	5	914 (5)	11
				899 (7)	-4	915 (7)	12	912 (9)	9	904 (3)	1	901 (5)	-2
				897 (4)	-6	908 (5)	5	909 (4)	6	902 (4)	-1	898 (4)	-5

655

656

Dr. Sophie Sobanska
CNRS Researcher
ISM UMR CNRS 5255 – Université de Bordeaux
Bât A12, 351 cours de la Libération
33405 Talence, France
Tel: +33 5 40 00 31 88
E-mail: sophie.sobanska@u-bordeaux.fr

February 20th, 2021

Credit author statement

Ref : MS MOLSTRUC-D-20-05163
Title "**Infrared matrix-isolation and theoretical studies of interactions between CH_3I and water.**" as a regular research paper in **Journal of Molecular Structure.**
Authors: Sophie Sobanska, Hanaa Houjeij, Stéphane Coussan, Christian Aupetit, Sonia Taamalli, Florent Louis, Laurent Cantrel, Anne Cécile Gregoire, Joëlle Mascetti

We declare that the work was carried out by all the authors associated with the manuscript. The tasks were distributed as follows:

S. Sobanska is the PI of the project and the corresponding authors. She participates to the interpretation of the experimental results and writing of the manuscript.
S. Coussan and J. Mascetti conducted the matrix experiments, help in the interpretation of the experimental and theoretical results and writing of the manuscript.
H. Houjeij, C. Aupetit did the matrix experiments
S. Taamalli and F. Louis did the theoretical calculations
AC Gregoire and L. Cantrel participates to the global project and read the final manuscript version

Declaration of interests

☒ The authors declare that they have no known competing financial interests or personal relationships that could have appeared to influence the work reported in this paper.

☐The authors declare the following financial interests/personal relationships which may be considered as potential competing interests:

Sophie Sobanska